Exploring the Reactivity of α-Acetamidocinnamic Acid and 4-Phenylpyridine with Zn(II) and Cd(II)

Daniel Ejarque[a], Francisco Sánchez-Férez[a], Teresa Calvet[b] , Mercè Font-Bardia[c] and Josefina Pons[a,*]

[a]Departament de Química, Universitat Autònoma de Barcelona, 08193-Bellaterra, Barcelona, Spain

[b]Mineralogia, Petrologia i Geologia Aplicada, Universitat de Barcelona, Martí i Franquès s/n, 08028 Barcelona, Spain

[c]Unitat de Difracció de Raig-X, Centres Científics i Tecnològics de la Universitat de Barcelona (CCiYUB), Universitat de Barcelona, Solé i Sabarís, 1-3, 08028 Barcelona, Spain

[*]Corresponding author E-mail: josefina.pons@uab.es

Abstract

The synthesis and characterization of four new coordination complexes is presented. Two of them have been obtained by reaction between $M(OAc)_2 \cdot 2H_2O$ (M= Zn(II), Cd(II)) and α-acetamidocinnamic acid (HACA) yielding two isostructural monomeric compounds with general formula $[M(ACA)_2(H_2O)_2]$ (M=Zn(II) (**1**), Cd(II) (**2**)). In opposite, the reactivity of **1** and **2** with 4-phenylpyridine (4-Phpy) leads to a monomeric $[Zn(4\text{-}Phpy)_2(ACA)_2(H_2O)_2] \cdot 3H_2O$ (**3**) or a dimeric compound $[Cd(4\text{-}Phpy)_2(\mu\text{-}ACA)(ACA)]_2 \cdot 2EtOH$ (**4**). All of them have been characterised by analytical and spectroscopic techniques. In addition, single crystals of **1**-**4** for X-ray diffraction

analysis have been obtained and their intra- and intermolecular interactions have been discussed and studied by Hirshfeld surface analysis, showing 3D supramolecular networks for all the compounds. In addition, the thermal stability of **3** and **4** has been studied. Finally, the photoluminescence properties of **1**-**4** have been examined, and their quantum yields calculated.

Keywords: α-acetamidocinnamic acid; 4-phenylpyridine; Zn(II); Cd(II); X-ray diffraction; quantum yield

1. Introduction

During the last decades, coordination complexes have been extensively studied for their wide structural variety and their potential applications in the field of sensing[1], luminescence[2], gas storage[3] and so on[4–6]. Recently, a new class of coordination complexes, supramolecular metal-organic frameworks (SMOFs), have been used to synthesise porous materials based on intermolecular interactions[7–10]. These complexes present properties that outperform those of the porous materials whose arrays are constructed through coordination bonds (metal-organic frameworks, MOFs), such as solvent processability, high thermal stability, easy purification, mild reaction conditions and regeneration by simple recrystallization[11,12].

The strategy for the synthesis of SMOFs is based on the preparation of discrete metal complexes using ligands which facilitate several weak interactions between rigid molecular units engaged by self-assembly[13]. Self-assembly has been demonstrated to be a robust tool based on the hierarchical association of the ligands according to the strongest supramolecular interactions[14,15]. These interactions, which direct the propagation of the structure are key factors for the design of SMOFs [16,17].

Above all the ligands, carboxylic acids have been employed as multifunctional tectons not only for their ability to coordinate to metal ions through a large diversity of coordination modes, but also for their labile nature[18] (Figure 1). Among them, cinnamic acid (HCA) and its derivatives have attracted a great interest for their photoluminescence[19], magnetic[20] and pharmacological properties (antibacterial, antifungal, antiparasitic[21], anti-inflammatory[22] and anti-oxidant[23]). Because of these properties, several compounds have been synthesised containing alkali[24,25], alkaline earth[26,27], Mn(II)[28], Co(II)[29,30], Ni(II)[31,32], Cu(II)[33–35], Pb(II)[36] or rare-earth[20,37,38] metal ions.

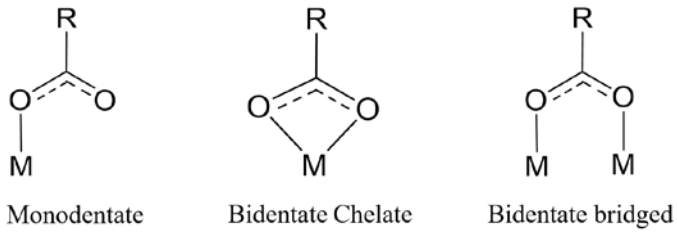

Figure 1. Coordination modes of the carboxylate ligand present in this work. M = metal atom.

Among all the metal ions, those with d^{10} electronic configuration are particularly interesting for their great variety of coordination numbers and arrangements[39]. In addition, d^{10} metal ions, having zero crystal field stabilization energy, implies weak coordination bonds and allows the reorganization of the ligands resulting in highly ordered arrays. Concretely, numerous Zn(II) and Cd(II) complexes have been synthesised yielding monomeric[40,41], dimeric[42,43] or polymeric[44,45] species such as $[Zn(2\text{-py-in})_2(THF)]$[40] (2-py-in = 2-(2-pyridyl)indole, THF = tetrahydrofuran), $[Zn(\mu\text{-pz})(pzH)(O_2CCH_2CH_3)]_2$[42] (pzH = pyrazole) or $[Cd(phen)(\mu\text{-}NO_3)_2(H_2O)]_n$[45] (phen = 1,10-phenantroline). Zn(II) and Cd(II) ions can adopt different coordination geometries from tetrahedral to octahedral, being the tetrahedral

the most common for Zn(II) ions[46] and the octahedral for Cd(II) ions[47], mainly for their M(II) ionic radius.

Cinnamic acid and derivatives are conjugated ligands where the carboxylic group is connected with the aromatic ring by a double bond. For these reason, they present promising photoluminescent properties. In these sense, some luminescent coordination compounds using Zn(II) and Cd(II) with HCA or 4-dimethylamino cinnamate (4-DACA) as ligands were previously described in the literature, $[Zn(phen)(4\text{-}DACA)_2]$[48] and $[Cd(bpy)(CA)_2(H_2O)]$[49] (bpy = 2,2'- bipyridine), studying their solution and solid-state photoluminescence properties and calculating their quantum yields. These studies show that the enhancement of the photoluminescence properties of the complexes respect to the ligands and their shift on the position of emission may be due to their coordination, which increase the rigidity of the ligands and reduce their loss of energy in other undesired processes.

Previously, our group has focused on the synthesis of copper complexes with cinnamic acid derivative ligands in combination with different pyridine derivatives (dPy = 4-*tert*-butylpyridine (4-^{t}Bupy), 4-acetylpyridine (4-Acpy), 3-phenylpyridine (3-Phpy) and 4-phenylpyridine, (4-Phpy)) using MeOH as solvent at r.t. These set of reactions yielded monomeric, dimeric and polymeric species such as $[Cu(4\text{-}Phpy)_2(p\text{-}OHCA)_2]$, $[Cu(4\text{-}Phpy)_2(\mu\text{-}p\text{-}OHCA)(p\text{-}OHCA)]_2$ and $[Cu(\mu\text{-}p\text{-}OHCA)_2(4\text{-}\ Acpy)_2]_n$. Interestingly, the compounds containing 4-Phpy undergo a photoinduced process[33].

As a continuation, we focused on the study of another cinnamic acid derivative, α-acetamidocinnamic acid (HACA). This ligand is used as a precursor in the formation of the L-phenylalanine amino acid[50] and has been mainly employed as a substrate for

the catalytic asymmetric hydrogenation of its double bond[51,52]. To the best of our knowledge, there are not previously reported complexes using HACA ligand.

In this contribution, we have assayed reactions between $M(OAc)_2 \cdot 2H_2O$ (M = Zn(II) and Cd(II)) and HACA acid, obtaining two isostructural monomeric compounds, $[Zn(ACA)_2(H_2O)_2]$ (**1**) and $[Cd(ACA)_2(H_2O)_2]$ (**2**). In opposite, the addition of the 4-phenylpyridine (4-Phpy), yields compounds with different nuclearity despite the precursor present the same structure. From the reaction between **1** and 4-Phpy, the monomeric $[Zn(4\text{-Phpy})_2(ACA)_2(H_2O)_2] \cdot 3H_2O$ (**3**) compound is obtained, while the reaction between **2** and 4-Phpy yields a dimeric compound, $[Cd(4\text{-Phpy})_2(\mu\text{-}ACA)(ACA)]_2 \cdot 2EtOH$ (**4**) (Scheme 1). All these set of compounds were fully characterised by analytical and spectroscopic techniques. Photophysical properties for all the complexes were analysed and their quantum yields calculated.

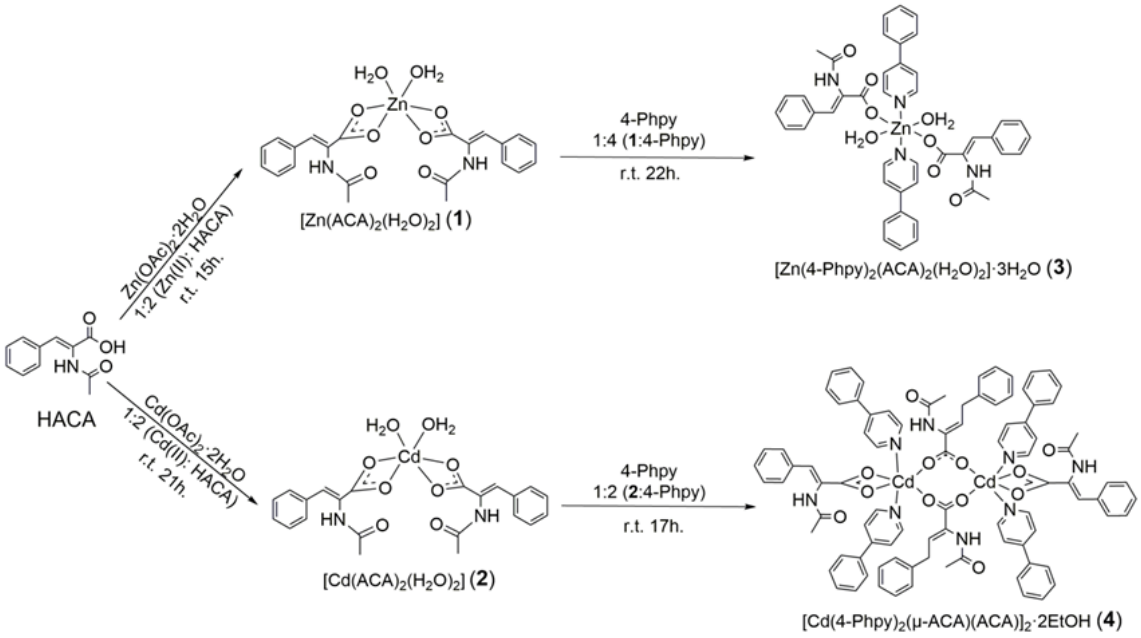

Scheme 1. Outline of the synthesis of compounds **1**-**4**.

2. Results and discussion

2.1. Synthesis and general characterization

Two monomeric compounds (**1** and **2**) were obtained by the direct reaction of $M(OAc)_2 \cdot 2H_2O$ (M = Zn(II) and Cd(II)) with α-acetamidocinnamic acid (HACA) in a 1:2 molar ratio. The reaction of **1** with 4-Phpy in a 1:4 molar ratio yields a monomeric complex (**3**). By contrast, the combination of **2** with 4-Phpy in a 1:2 molar ratio yields a dimeric compound (**4**). All these reactions have been performed using EtOH as solvent at room temperature (r.t.). In addition, single crystals for X-ray diffraction method were grown by slow evaporation of mother liquors at r.t. for **1** and **2**, and at low temperature (4 ºC) for **3** and **4**.

Compounds **1-4** were characterised by elemental analysis, FTIR-ATR, ^{1}H and $^{13}C\{^{1}H\}$ NMR spectroscopies and single crystal X-ray diffraction method. In addition, TG/DTA determinations of compounds **3** and **4** were recorded. Finally, the UV-Vis and photoluminescence properties of compounds **1-4** were analysed and their quantum yields calculated.

The elemental analysis of compounds **1-4** agrees with the proposed formula. The FTIR-ATR spectra of **1-4** show the characteristic bands of the carboxylate between 1609 and 1509 cm^{-1} for $\nu_{as}(COO)$ and between 1450 and 1387 cm^{-1} for $\nu_{s}(COO)$. The difference between these bands [$\Delta = \nu_{as}(COO) - \nu_{s}(COO)$][53,54] is 111 and 62 cm^{-1} (**1**), 88 and 64 cm^{-1} (**2**), 217 cm^{-1} (**3**) and 174 and 125 cm^{-1} (**4**) suggesting monodentate (**3**), chelate (**1**, **2**) and chelate and bridged (**4**) coordination modes of the carboxylate ligands (S.I: Figures S1-S4). The bands attributable to the aromatic groups $\nu(C\text{-}H)_{ar}$, $\nu(C=C/C=N)$, $\delta(C\text{-}H)_{ip}$, and $\delta(C\text{-}H)_{oop}$ are also identified[55].

The presence of solvent molecules allows further identification of some specific bands. Compounds **1-4** present peaks assignable to ν(O-H) of water (**1-3**) or ethanol (**4**) molecules in the range of 3383-3201 cm^{-1}. In addition, all the compounds exhibit a peak

attributable to ν(N-H) between 3298 and 3212 cm^{-1}. Therefore, the FTIR-ATR spectral data agree with the structures determined by single crystal X-ray diffraction method.

The ^{1}H and $^{13}C\{^{1}H\}$ NMR spectra of complexes **1**-**4** have been recorded in dmso-d_6 solution. In the ^{1}H NMR spectra of compounds **1**-**4**, the signals attributable to the N*H* groups of the ACA ligand appeared between 9.21 and 9.18 ppm. The aromatic protons of the ACA ligand show signals between 7.52 and 7.28 ppm while the alkene protons are present between 7.33 and 7.24 ppm. Finally, the aliphatic protons exhibit a signal between 1.96 and 1.95 ppm (free HACA: 9.47, 7.61-7.38, 7.21 and 1.98 ppm). The ^{1}H NMR spectra confirm the coordination of the ACA ligand to the metal centres (S.I: Figures S5-S8). In addition, complexes **3** and **4** display the signals attributable to the aromatic protons of the 4-Phpy ligand between 8.65 and 7.51 ppm (free 4-Phpy: 8.64-7.50 ppm) (S.I: Figures S7 and S8). Furthermore, compound **4** presents signals corresponding to the occluded EtOH molecules at 4.35 (-O*H*), 3.44 (-CH_2-) and 1.05 (-CH_3) ppm with a shift of the -O*H* signal respect to the free EtOH molecules (4.63, 3.44 and 1.06 ppm), which is probably driven by intermolecular interactions (S.I: Figure S8). The ^{1}H NMR spectra of **3** and **4** confirms the 1:1 molar ratio of the ACA and 4-Phpy ligands.

In the $^{13}C\{^{1}H\}$ NMR spectra of complexes **1**-**4** the signals corresponding to the carbon atoms of the ACA and 4-Phpy ligands are present. In compounds **1**, **2** and **4**, the carbon atom from the C=O group appeared between 171.5 and 170.5 ppm. For all the compounds, the carboxylate groups display signals between 168.4 and 168.1 ppm. The quaternary alkene carbons are shown between 135.2 and 135.0 ppm and the aromatic carbons appeared between 129.7 and 128.3 ppm. Finally, the remaining alkene carbons are shown between 128.2 and 128.0 ppm and the aliphatic protons between 23.1 and 23.0 ppm (free HACA: 169.3, 166.4, 133.7, 132.2-128.8, 127.4, 23.6 ppm) (S.I: Figures

S9-S12). In addition, in compounds **3** and **4**, the spectra display signals attributable to the aromatic carbons of the 4-Phpy ligands between 150.3 and 121.4 ppm (free 4-Phpy: 149.9-123.1 ppm) (S.I: Figures S11 and S12). Moreover, in the spectrum of compound **4**, the aliphatic protons of the EtOH occluded molecules are observed at 56.1 ppm (for -CH_2-) and 18.6 ppm (for -CH_3) (S.I: Figure S12). The chemical shift of the peak assigned to the *C*OO group, suggest its coordination to the metal centre. Further NMR data is provided in the Experimental Section.

*2.2. Structural Description of [Zn(ACA)$_2$(H$_2$O)$_2$] (**1**) and [Cd(ACA)$_2$(H$_2$O)$_2$] (**2**)*

Compounds **1** and **2** belongs to the monoclinic C2/c space group. Both are isostructural compounds (S.I: Figure S13) where the metal atoms present a [MO_6] *core* (M = Zn(II) for **1** and Cd(II) for **2**). In both compounds, the metal centre is coordinated to four carboxylate oxygen atoms from two ACA ligands, which exhibit a chelate coordination mode, and two oxygen atoms from two water molecules with a *cis* disposition. The distortion on the geometry is evaluated through the average twist angle. While higher average twist angles around 60º belongs from octahedral geometry, lower values close to 0º pertains to a trigonal prism geometry[56,57]. Compounds **1** and **2** exhibit an average twist angle of 41.22° for **1** (O1-Cg1-Cg2-O2#1, 48.00°; O2-Cg1-Cg2-O1#1, 48.00°; O4-Cg1-Cg2-O4#1, 27.65°) and 36.36° for **2** (O1-Cg1-Cg2-O2, 26.37°; O4#1-Cg1-Cg2-O1, 55.73°; O4-Cg1-Cg2-O2#1, 26.98°), indicating distorted octahedral geometries. The values of M-O_{ACA} bond lengths range between 1.9953(10)-2.5309(10) Å (**1**) or 2.3301(9)-2.3602(8) Å (**2**), while the M-O_{water} bond distances present shorter lengths with a smaller (1.9903(10) Å, in **1**) or larger (2.2145(9) Å, in **2**) difference respect to the M-O_{ACA} bond lengths. The values of O-M-O bond angles are 71.21(3)-149.33(6)° for **1** and 56.01(3)-171.28(3)° for **2** (Tables 1 and 2; Figure 2).

Table 1. Selected bond lengths (Å), bond angles (°), twist angles (°) and intermolecular interactions (Å) for compound **1**.

Bond lengths (Å)			
Zn(1)-O(1)	1.9953(10)	Zn(1)-O(4)	1.9903(10)
Zn(1)-O(2)	2.5309(10)		
Bond angles (°)			
O(1)-Zn(1)-O(1)#1	149.33(6)	O(2)-Zn(1)-O(4)#1	147.10(4)
O(1)-Zn(1)-O(2)	56.74(4)	O(4)-Zn(1)-O(1)	107.00(4)
O(1)-Zn(1)-O(2)#1	96.81(4)	O(4)-Zn(1)-O(1)#1	93.14(4)
O(2)-Zn(1)-O(2)#1	71.21(3)	O(4)-Zn(1)-O(4)#1	97.99(6)
O(2)-Zn(1)-O(4)	103.14(4)		
Twist angles (°)			
O(1)-Cg(1)-Cg(2)-O(2)#1	48.00	O(4)-Cg(1)-Cg(2)-O(4)#1	27.65
O(2)-Cg(1)-Cg(2)-O(1)#1	48.00		

Intermolecular interactions (Å)				
D-H···A	D-H (Å)	H···A (Å)	D···A (Å)	> D-H···A (°)
N(1)-H(1N)···O(1)	0.84(2)	2.24(2)	3.0495(16)	160.8(18)
O(4)-H(4OB)···O(3)	0.806(14)	1.852(13)	2.6533(15)	173.1(17)
O(4)-H(4OA)···O(2)	0.805(13)	1.826(13)	2.6238(15)	170.7(17)
C(7)-H(7)···Cg(3)	0.95	2.96	3.7150(17)	137

#1: -x+1,-y,-z+1/2; Cg(1) = O(1) O(2) O(4); Cg(2) = O(1)#1 O(2)#1 O(4)#1; Cg(3) = C(6) C(7) C(8) C(9) C(10) (C11)

Table 2. Selected bond lengths (Å), bond angles (°), twist angles (°) and intermolecular interactions (Å) for compound **2**.

Bond lengths (Å)			
Cd(1)-O(1)	2.3301(9)	Cd(1)-O(4)	2.2145(9)
Cd(1)-O(2)	2.3602(8)		
Bond angles (°)			
O(1)-Cd(1)-O(2)	56.01(3)	O(4)#1-Cd(1)-O(1)	89.80(3)
O(1)#1-Cd(1)-O(1)	171.28(4)	O(4)#1-Cd(1)-O(1)#1	96.33(3)
O(1)#1-Cd(1)-O(2)	116.28(3)	O(4)#1-Cd(1)-O(2)	142.66(3)
O(2)-Cd(1)-O(2)#1	80.23(4)	O(4)#1-Cd(1)-O(4)	90.64(5)
O(4)-Cd(1)-O(2)	106.28(3)		
Twist angles (°)			
O(1)-Cg(1)-Cg(2)-O(2)	26.37	O(4)-Cg(1)-Cg(2)-O(2)#1	26.98
O(4)#1-Cg(1)-Cg(2)-O(1)	55.73		

Intermolecular interactions (Å)				
D-H···A	D-H (Å)	H···A (Å)	D···A (Å)	> D-H···A (°)
N(1)-H(1N)···O(1)	0.88	2.21	2.9782(13)	146
O(4)-H(4OB)···O(3)	0.786(19)	1.874(19)	2.6554(13)	173(2)
O(4)-H(4OA)···O(2)	0.82(2)	1.86(2)	2.6771(12)	172(2)
C(11)-H(11)···Cg(3)	0.95	3.45	4.1790(20)	135

#1: -x+1,-y,-z+1/2; Cg(1) = O(1) O(4) O(4)#1; Cg(2) = O(1)#1 O(2) O(2)#1; Cg(3) = C(6) C(7) C(8) C(9) C(10) (C11)

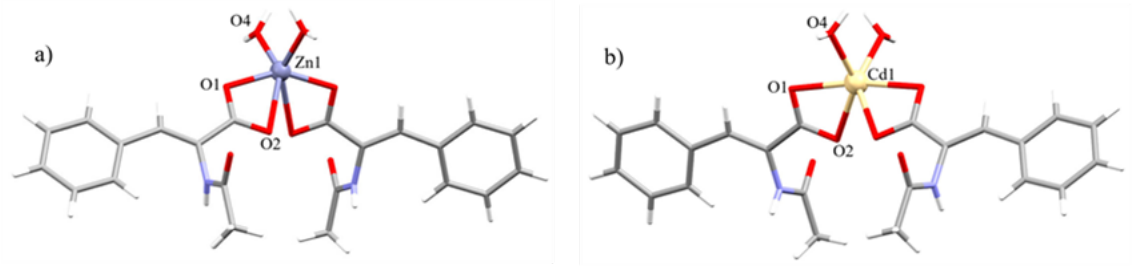

Figure 2. Molecular structure of compound a. **1** and b. **2**.

Compound **1** presents a larger Zn-O_{ACA} bond length (Zn-O_{ACA}, 2.5309(10) Å) compared with a complex with similar [ZnO_6] *core*, which also has two oxygen atoms belonging from water molecules and four oxygen atoms from carboxylate moieties: [$Zn(CA)_2(H_2O)_2$][58] (CA = cinnamate anion) (Zn-O_{CA}, 2.118(3)-2.390(3) Å). Similar values to the larger Zn-O_{ACA} bond length are also present in other compounds such as [$Zn(tdc)(4\text{-}bpmh)]_n \cdot n(H_2O)$[59] (tdc = 2,5-thiophene dicarboxylate, 4-bpmh = N,N-bis-pyridin-4-ylmethylene-hydrazine) (Zn-O_{ACA}, 1.951(1)-2.505(1) Å) and [$Zn(2,2'\text{-}bpy)(4\text{-}OHBz)_2(H_2O)$][60] (2,2'-bpy = 2,2'-bipyridine, 4-OHBz = 4-hydroxy benzoate) (Zn-O_{ACA}, 2.0045(14)-2.5300(15) Å; Zn-O_{water}, 2.1375(15) Å). According to these results, we can consider these association as a weak coordination bonds or semi-bonds[48]. Different from **1**, in compound **2** all the values of bond lengths and angles are similar to the analogous [$Cd(CA)_2(H_2O)_2$] compound (Cd-O_{CA}, 2.330(2)-2.375(2) Å; Cd-O_{water}, 2.208(2) Å; O-Cd-O, 55.96(7)-141.89(7)°)[61], displaying a chelated coordination mode with more symmetry and with bond lengths in a similar range than in **1**, which due to the bigger van der Waals radius of Cd(II) (1.58 Å) respect Zn(II) (1.39 Å), are considered as a standard coordination bond. Moreover, compound **2** presents a larger bond angle (O_{ACA}-Cd-O_{ACA}, 171.28(3)°) compared with [$Cd(CA)_2(H_2O)_2$] (O_{CA}-Cd-O_{CA}, 90.65(7)°), which could be promoted by the steric hindrance of the acetamide moiety of the ACA ligand.

The intermolecular interactions of the NH moieties of the ACA ligands are the same in **1** and **2**. In both compounds, the NH group acts as an H-bond donor exhibiting intermolecular interactions with an oxygen atom of the coordinated carboxylate group of other ACA ligand (**1**: N(1)-H(1N)···O(1), 2.24(2) Å; **2**: N(1)-H(1N)···O(1), 2.21(3) Å) and propagating the structure through the *b* axis. In addition, the two coordinated water molecules in **1** and **2** exhibit the same supramolecular behaviour. Both form two H-bond interactions: one with the C=O group of a neighbouring monomeric unit (**1**: O(4)-H(4OB)···O(3), 1.852(13) Å; **2**: O(4)-H(4OB)···O(3), 1.874(19) Å) and the other with a coordinated oxygen atom of a carboxylate group from another molecule (**1**: O(4)-H(4OA)···O(2), 1.826(13) Å; **2**: O(4)-H(4OA)···O(2), 1.86(2) Å). All these set of interactions expand the structure forming 2D layers along the *bc* plane (Tables 1 and 2; Figure 3).

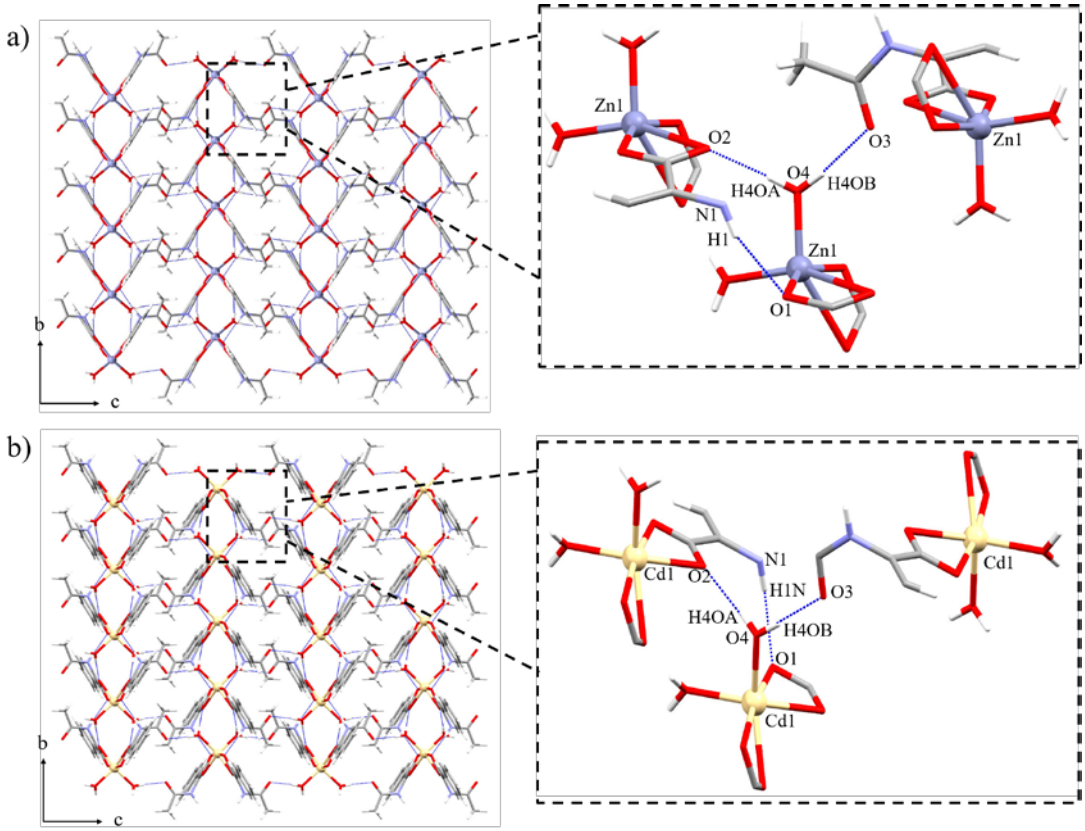

Figure 3. Supramolecular 2D expansion along the *bc* plane in compounds a. **1** and b. **2**.

In addition, both compounds present C-H···π interactions between the aromatic *o*-H with a nearby aromatic ring from a neighbouring monomeric unit (**1**: C(7)-H(7)···Cg(3), 2.96 Å; **2**: C(11)-H(11)···Cg(3), 3.45 Å), extending their structures along the *a* axis and forming 3D nets (Figure 4).

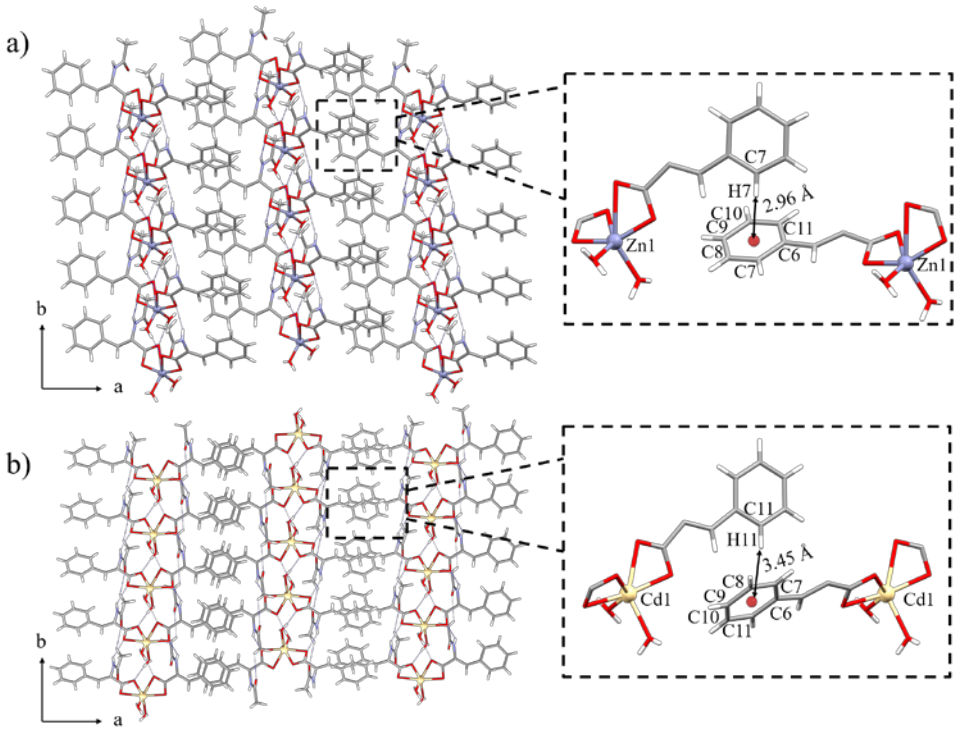

Figure 4. Supramolecular 2D expansion along the *ab* plane in compounds a. **1** and b. **2**

*2.3. Structural Description of [Zn(4-Phpy)$_2$(ACA)$_2$(H$_2$O)$_2$]·3H$_2$O (**3**)*

Compound **3** belongs to the monoclinic P2$_1$/n space group. It consists of Zn(II) monomers with a [ZnN$_2$O$_4$] *core*. The metal centre is coordinated by two nitrogen atoms from two 4-Phpy ligands, two carboxylate oxygen atoms from two ACA ligands, which exhibit two monodentate coordination modes, and two oxygen atoms from two water molecules, displaying a distorted octahedral geometry with an average twist angle of 60.00° (O1-Cg1-Cg2-N2#1, 57.58°; N2-Cg1-Cg2-O4#1, 62.06°; O4-Cg1-Cg2-O1#1, 60.36°) (Table 3; Figure 5a). It is noteworthy to mention the *trans* disposition of all the ligands in comparison with **1**.

Table 3. Selected bond lengths (Å), bond angles (°), twist angles (°) and intramolecular and intermolecular interactions (Å) for compound **3**.

Bond lengths (Å)				
Zn(1)-N(2)		2.134(2)	Zn(1)-O(4)	2.1352(17)
Zn(1)-O(1)		2.1436(17)		
Bond angles (°)				
N(2)-Zn(1)-N(2)#1		180.0	N(2)-Zn(1)-O(4)	85.01(7)
O(4)-Zn(1)-O(4)#1		180.0	N(2)-Zn(1)-O(1)#1	89.70(7)
N(2)-Zn(1)-O(1)		90.30(7)	O(1)#1-Zn(1)-O(1)	180.0
O(4)-Zn(1)-O(1)		93.39(6)	N(2)-Zn(1)-O(4)#1	94.99(8)
O(4)#1-Zn(1)-O(1)		86.61(6)	Phenyl-Pyridil (4-Phpy)	7.18
Twist angles (°)				
O(1)-Cg(1)-Cg(2)-N(2)#1		57.58	O(4)-Cg(1)-Cg(2)-O(1) #1	60.36
N(2)-Cg(1)-Cg(2)-O(4) #1		62.06		
Intramolecular interactions (Å)				
D-H···A	D-H (Å)	H···A (Å)	D···A (Å)	> D-H···A (°)
O(4)-H(4OB)···O(2)	0.80(3)	1.80(2)	2.604(3)	173(2)
Intermolecular interactions (Å)				
D-H···A	D-H (Å)	H···A (Å)	D···A (Å)	> D-H···A (°)
N(1)-H(1)···O(2)	0.88	2.04	2.840(3)	151
C(11)-H(11C)···O(3)	0.98	2.51	3.262(3)	134
C(11)-H(11A)···Cg(3)	0.98	2.78	3.655(3)	149
O(4)-H(4OA)···O(1)	0.80(2)	2.084(19)	2.838(2)	158(3)
C(12)-H(12)···O(4)	0.95	2.54	3.425(3)	155
C(7)-H(7)···O(3)	0.95	2.52	3.414(5)	157
C(20)-H(20)···O(2)	0.95	2.61	3.32(1)	132

#1: -x+1,-y+1,-z+1; Cg(1) = N(2) O(1) O(4); Cg(2) = N(2)#1 O(1)#1 O(4)#1; Cg(3) = N(2) C(12) C(13) C(14) C(15) C(16).

The two Zn-O_{ACA} bonds lengths are 2.1436(17) Å while the two Zn-N bonds lengths are 2.134(2) Å and are similar to other complexes reported in the literature, which contain pyridine derivative ligands and monodentate carboxylates coordinated to Zn(II) ions[62,63], such as $\{(acrH)_2\text{-}[Zn(pyzdc)_2]\}_n$[62] (acrH = acridinium cation; pyzdc = pyrazine-2,3-dicarboxylate) (Zn-O_{pyzdc}, 2.0326(17)-2.2435(17) Å; Zn-N_{pyzdc}, 2.093(2) Å), $[Zn(tpy)(pydc)]\cdot 4H_2O$[63] (tpy = 2,2′:6′,2″-terpyridine; pydc = pyridine-2,6-dicarboxylate) (Zn-O_{pydc}, 2.138(3)-2.268(3) Å; Zn-N, 2.020(3)-2.173(3) Å). In addition, the Zn-O_{water} bond length is 2.1352(17) Å, which is similar to other complexes with coordinated water molecules such as $[Zn(IH)_2(H_2O)_4](NO_3)_2$[64] (IH = isonicotinoylhydrazone) (Zn-O_{water}, 2.0816(19)-2.1356(18) Å) and

{[Zn(gly)$_2$(H$_2$O)$_4$][Zn(H$_2$O)$_6$](SO$_4$)}[65] (Zn-O$_{water}$, 2.0320(13)-2.1332(13) Å). The values of O-Zn-O bond angles are between 86.61(6) and 93.39(3)° and the O-Zn-N between 85.01(7) and 94.99(8)°. In this compound, the 4-Phpy present a torsion angle between their pyridyl and phenyl rings of 7.18° showing a small deviation from planarity (Table 3).

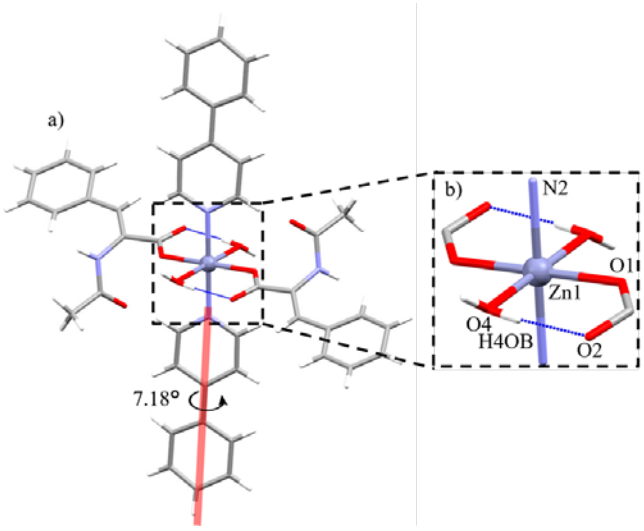

Figure 5. a. Molecular structure of **3**. b. In detail view of the intramolecular H-bond interactions.

The intramolecular interactions of **3** are based on strong H-bond interactions of the coordinated water molecules through one of its hydrogen atoms with the oxygen atoms of the uncoordinated carboxylate from the ACA ligands (O(4)-H(4OB)···O(2), 1.80(2) Å) (Figure 5b).

The intermolecular interactions of the ACA ligands and the coordinated water molecules in **3** expand the structure along the *b* axis, forming a supramolecular 1D chain (Table 3; Figure 6a). The ACA ligands act as H-bond donor through the NH and the CH$_3$ groups of the same monomer, promoting two intermolecular interactions with the oxygen atoms of a carboxylate and a carbonyl group of another molecule (N(1)-H(1)···O(2), 2.04 Å; C(11)-H(11C)···O(3), 2.51 Å) (Figure 6b). In addition, the CH$_3$ moieties interact with the aromatic ring from another monomeric unit through a C-H···π

interaction (C(11)-H(11A)···Cg(3), 2.78 Å). Moreover, the two coordinated water molecules exhibit the same supramolecular behaviour, displaying one H-bond interaction with an oxygen atom from a carboxylate group from a nearby molecule (O(4)-H(4OA)···O(1), 2.084(19) Å). Furthermore, the same water molecules exhibit other intermolecular interaction with an *o*-H atom from a 4-Phpy ligand coordinated to the same neighbouring molecule (C(12)-H(12)···O(4), 2.54 Å) (Figure 6c).

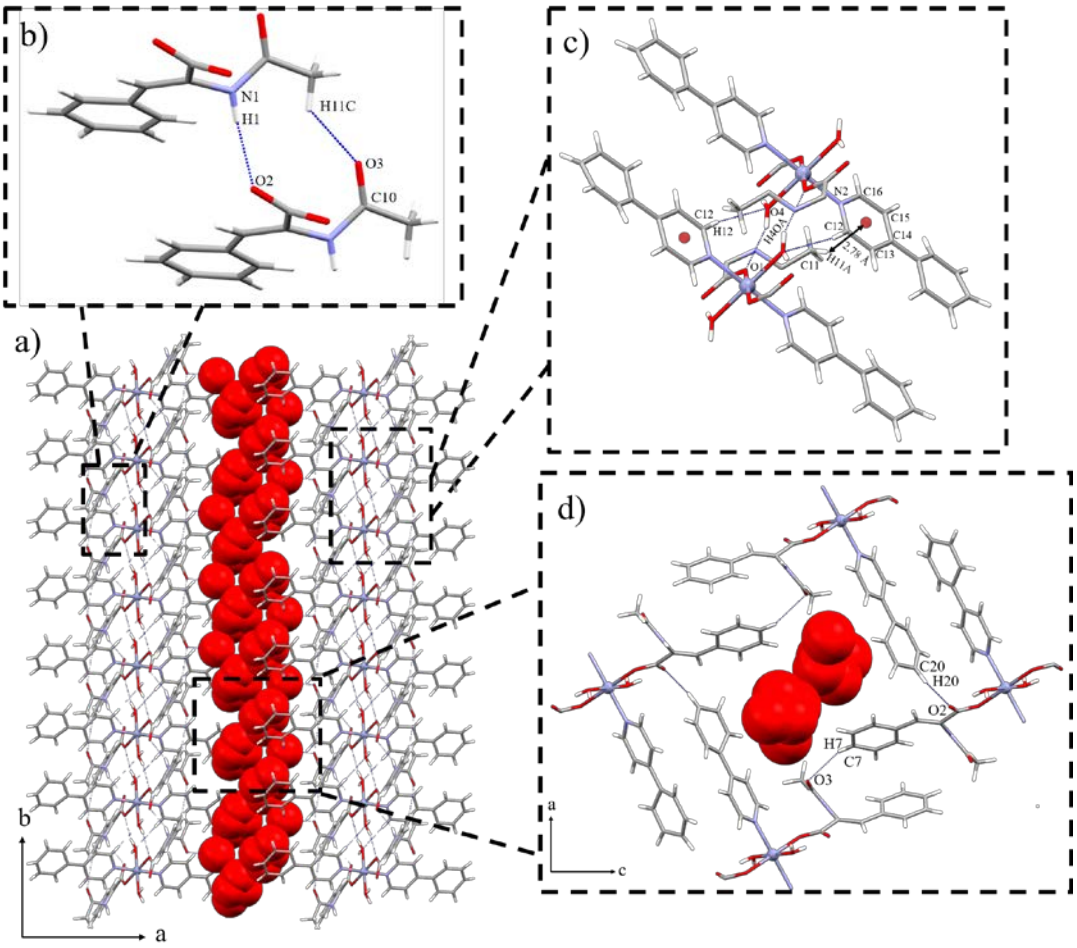

Figure 6. a. General view of the supramolecular chains along the *b* axis in **3**. In detail view of the interactions of b. ACA ligands, c. H_2O molecules and ACA ligands and d. Square-shape voids containing the occluded water molecules.

Finally, the structure is expanded through two C-H···O interactions along the *ac* plane, forming square-shaped voids[66] in which three disordered water molecules are occluded. These water molecules, occupy channels along the *b* direction generating an accessible volume of 7.5% (174.09 $Å^3$, calculated using a probe radius of 1.2 Å)[67].

One of the C-H···O interactions is performed by the ACA ligand through its *p*-H atoms with the carbonyl oxygen atom of a neighbouring molecule (C(7)-H(7)···O(3), 2.52 Å). The second C-H···O interaction, is promoted by the *p*-H of the phenyl ring from a 4-Phpy ligand of a third molecule with the oxygen atom of an uncoordinated carboxylate group of the ACA ligand from the same molecule which acts as H-bond donor in the previous hydrogen bond interaction (C(20)-H(20)···O(2), 2.61 Å) (Figure 6d). These interactions expand the structure along the *ac* plane and form a 3D network.

*2.4. Structural Description of [Cd(4-Phpy)$_2$(μ-ACA)(ACA)]$_2$·2EtOH (**4**).*

Compound **4** belongs to the monoclinic $P2_1/n$ space group. It consists of Cd(II) dimeric units with a [CdN_2O_4] *core*, composed by four ACA ligands and four 4-Phpy ligands (Figure 7a). Two of the ACA ligands display a bidentate chelate coordination mode while the other two show a bridging coordination mode, connecting the two metal ions of the dimeric unit. The six coordination environment of each metal is completed with two coordinated 4-Phpy ligands in *trans* disposition. Both Cd(II) centres display a distorted octahedral geometry with an average twist angle of 58.00° (O2-Cg1-Cg2-O5, 68.02°; O1-Cg1-Cg2-N4, 45.78°; N3-Cg1-Cg2-O4, 60.20°) (Table 4; Figure 7b).

The chelate bond lengths are 2.3420(18) and 2.4851(18) while the bridged are 2.2202(17) and 2.2241(19) Å and the Cd-N bond distances are between 2.301(2) and 2.310(2) Å. These values are similar to other complexes reported in the literature containing bridged and chelate carboxylate groups and pyridine derivative ligands coordinated to Cd(II) metal ions, such as [Cd(μ_3-opda)(μ-abpy)$_{0.5}$(H_2O)]$_n$[68] (opda = 1,2-phenylenediacetate; abpy = 4,4′-azobis(pyridine)) (Cd-N, 2.345(14) Å; Cd-$O_{chelated}$, 2.344(22)-2.426(13) Å; Cd-$O_{bridged}$, 2.283(10)-2.308(12) Å), [Cd$(OAc)_2$(4-DMAP)$_3$]·$2H_2O$[69] (4-DMAP = 4-dimethylaminopyridine) (Cd-N, 2.324(4)-2.333(3)

Å; Cd-$O_{chelated}$, 2.360(3)-2.591(3) Å) or $[Cd_2(\mu_2\text{-}OAc)_4(3\text{-}Mepy)_2]_n$[69] (3-Mepy = 3-methylpyridine) (Cd-N, 2.304(2)-2.318(2) Å; Cd-$O_{bridged}$, 2.185(3)-2.292(2) Å). The values of O-Cd-O bond angles are between 54.51(6)° and 115.18(8)° and the N-Cd-O bond angles between 85.09(7)° and 94.77(7)°. Moreover, the 4-Phpy ligands present torsion angles of 25.20° and 27.91°, indicating the high deviation from planarity of the 4-Phpy ligand in this compound. (Table 4)

Table 4. Selected bond lengths (Å), bond angles (°), twist angles (°) and intramolecular and intermolecular interactions (Å) for compound **4**.

Bond lengths (Å)			
Cd(1)-N(3)	2.310(2)	Cd(1)-O(2)	2.4851(18)
Cd(1)-N(4)	2.301(2)	Cd(1)-O(4)	2.2202(17)
Cd(1)-O(1)	2.3420(18)	Cd(1)-O(5)	2.2241(19)
Bond angles (°)			
N(3)-Cd(1)-O(1)	87.26(7)	N(3)-Cd(1)-O(2)	91.05(7)
N(4)-Cd(1)-N(3)	174.29(8)	N(4)-Cd(1)-O(1)	87.08(7)
N(4)-Cd(1)-O(2)	85.09(7)	O(1)-Cd(1)-O(2)	54.51(6)
O(4)-Cd(1)-N(3)	88.24(7)	O(4)-Cd(1)-N(4)	93.40(7)
O(4)-Cd(1)-O(1)	99.66(7)	O(4)-Cd(1)-O(2)	154.16(7)
O(4)-Cd(1)-O(5)#1	115.18(8)	O(5)#1-Cd(1)-N(3)	89.47(7)
O(5)#1-Cd(1)-N(4)	94.77(7)	O(5)#1-Cd(1)-O(1)	144.88(7)
O(5)#1-Cd(1)-O(2)	90.63(7)	Phenyl(1)-Pyridil(1) (4-Phpy)	25.20
Phenyl(2)-Pyridil(2) (4-Phpy)	27.91		
Twist angles (°)			
O(2)-Cg(1)-Cg(2)-O(5)	68.02	N(3)-Cg(1)-Cg(2)-O(4)	60.20
O(1)-Cg(1)-Cg(2)-N(4)	45.78		

Intramolecular interactions (Å)				
D-H···A	D-H (Å)	H···A (Å)	D···A (Å)	> D-H···A (°)
C(23)-H(23)···O(3)	0.95	2.36	3.197(4)	148
C(27)-H(27)···Cg(3)	0.95	2.65	3.497(3)	149

Intermolecular interactions (Å)				
D-H···A	D-H (Å)	H···A (Å)	D···A (Å)	> D-H···A (°)
N(1)-H(1N)···O(6)	0.88	2.00	2.799(3)	150
C(37)-H(37)···O(1)	0.95	2.43	3.338(3)	159
C(44)-H(44)···O(1)	0.95	2.47	3.375(3)	159
O(1W)-H(1W)···O(2)	0.79(3)	1.93(3)	2.704(3)	170(2)
N(2)-H(2N)···O(1W)	0.78(3)	2.14(3)	2.900(4)	165(3)
C(41)-H(41)···O(1W)	0.95	2.59	3.436(3)	149
C(18)-H(18)···O(3)	0.95	2.40	3.229(4)	146

#1: -x+1,-y+1,-z+1; Cg(1) = N(3) O(1) O(2); Cg(2) = N(4) O(4) O(5); Cg(3) = N(4) C(34) C(35) C(36) C(37) C(38)

The intramolecular interactions of **4** are promoted by the C=O group of the chelate ACA ligands, which interact with the *o*-H of the pyridyl ring of the 4-Phpy unit through a C-H···O interaction (C(23)-H(23)···O(3), 2.36 Å). The same 4-Phpy ligand also has a C-H···π interaction *via* its other *o*-H atom, with a pyridyl aromatic ring of a neighbouring 4-Phpy of the same dimeric unit (C(27)-H(27)···Cg(3), 2.65 Å) (Figure 7c).

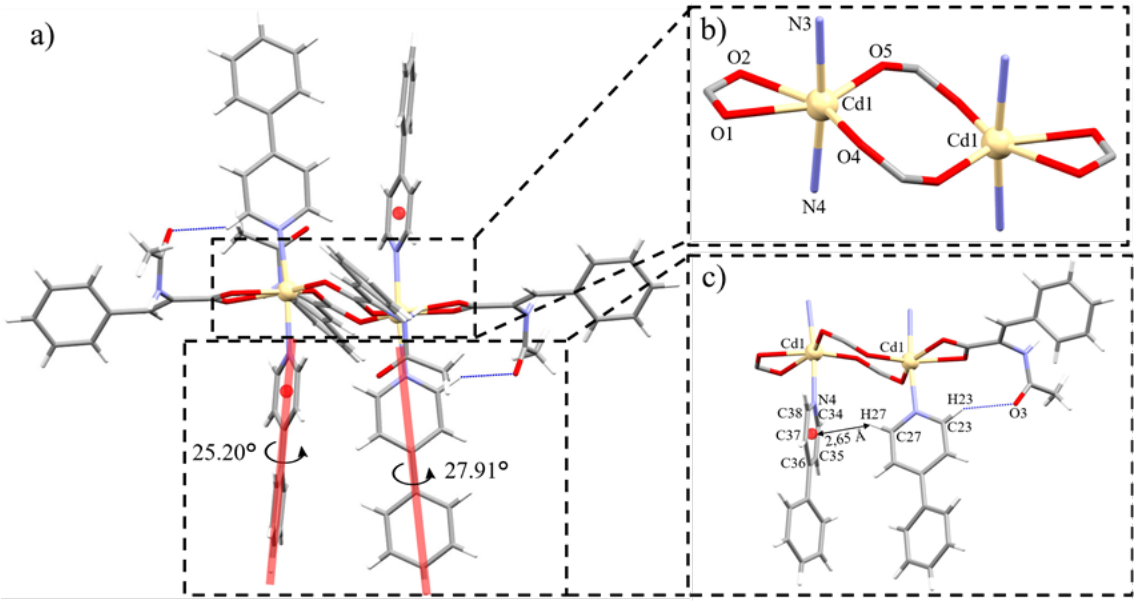

Figure 7. a. Molecular structure of **4**. In detail, view of *b*. Cd(II) *cores* and c. Intramolecular interactions.

The ACA ligands also act as H-bond donors exhibiting intermolecular interactions through their NH groups with the oxygen atoms of the C=O group of other ACA ligands (N(1)-H(1N)···O(6), 2.00 Å). In addition, the 4-Phpy ligands interact through their *m*-H of the phenyl ring and their *o*-H of the pyridyl ring of the same ligand with the oxygen atom of a carboxylate group from an ACA ligand of a neighbouring dimeric units (C(37)-H(37)···O(1), 2.43 Å; C(44)-H(44)···O(1), 2.47 Å). These interactions expand the structure forming a chain along the *a* axis (Figure 8).

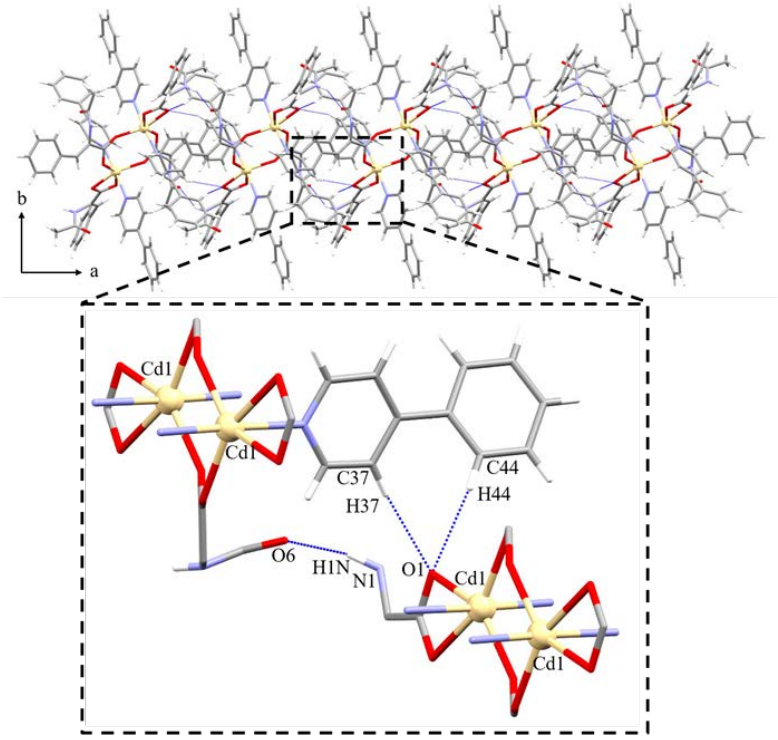

Figure 8. Supramolecular chains of **4** along the *a* axis. In detail, view of the N-H···O hydrogen bond and C-H···O interactions.

Furthermore, the structure expands along the *bc* plane through two occluded EtOH molecules for each dimeric unit, which interact with the dimers through three H-bond interactions (Figure 9a). The strongest H-bond interaction is promoted by the hydrogen atoms of the OH group from the EtOH molecules with an oxygen atom of a chelated carboxylate group from an ACA ligand of a neighbouring dimer (O(1W)-H(1W)···O(2), 1.93(3) Å). The oxygen atom of the occluded EtOH molecules also exhibit another H-bond interaction together with the NH group of the same dimeric unit (N(2)-H(2N)···O(1W), 2.14(3) Å). Finally, the oxygen atom of the occluded EtOH molecules display a weak H-bond with a *m*-H atom of a 4-Phpy ligand of another dimeric unit (C(41)-H(41)···O(1W), 2.59 Å) (Figure 9b). Moreover, there is a C-H···O interaction between the *p*-H atom of an ACA ligand and the oxygen atom of a C=O group from a neighbouring ACA ligand (C(18)-H(18)···O(3), 2.40 Å) (Figure 9c). All these set of interactions form a 3D supramolecular network.

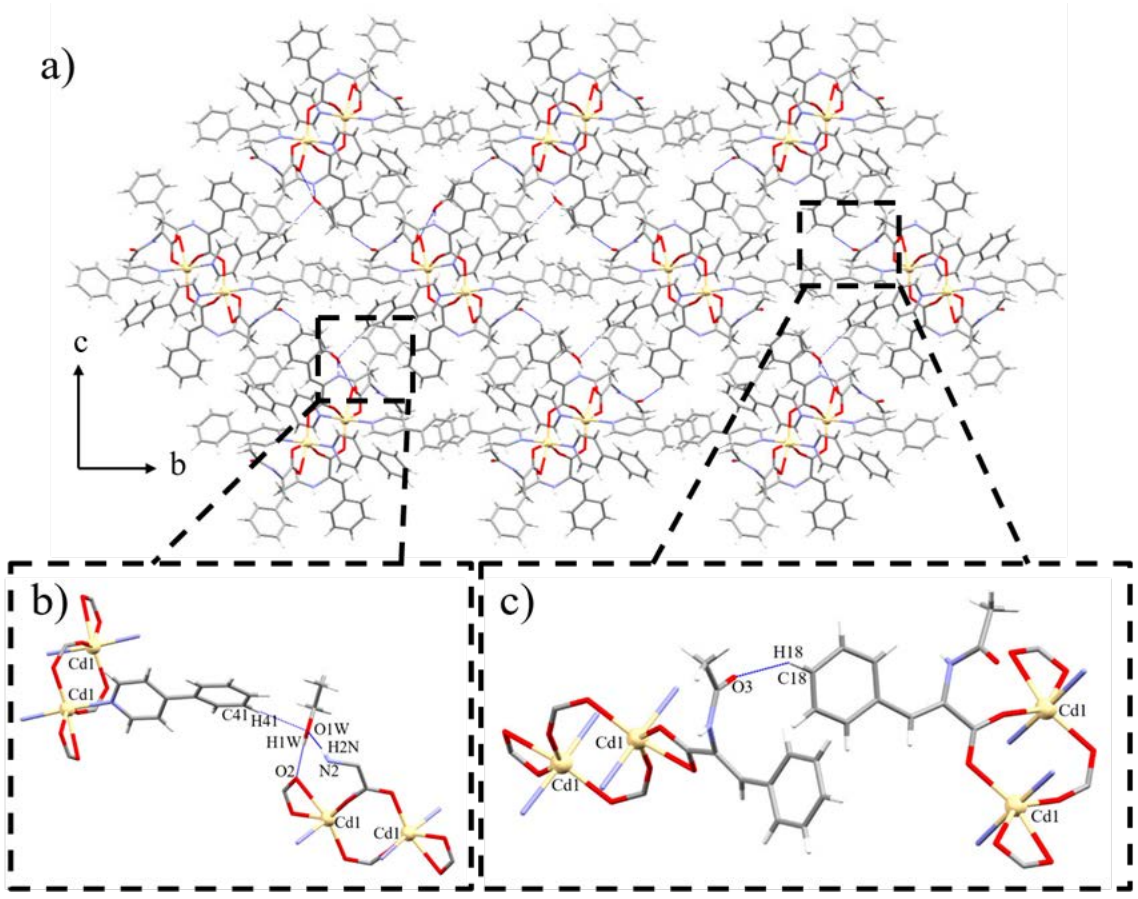

Figure 9. a. General view of the supramolecular plane formed along the *bc* plane in **4**. In detail, view of b. Intermolecular interactions of the EtOH molecules. c. C-H···O interactions of the ACA ligands.

2.5. Hirshfeld Surface Analysis

Hirshfeld surface analysis of complexes **1**-**4** have been performed with CrystalExplorer 2.1[70]. All the surfaces have been calculated at an isovalue of 0.5 e·au^{-3}.

Hirshfeld surfaces, in combination with 2D fingerprint plots, are a powerful graphical tool to evaluate supramolecular interactions present in crystal structures. The surface mapping facilitates their identification while the fingerprint plot outlines the distances between the atoms involved in these contacts.

The main associations present in compounds **1** and **2** are identified and highlighted (S.I: Figure S14a). They consists on four H-bonds between the amine units

and the carboxylate oxygen atoms (N-H···O_{COO}) and eight H-bonds of the water molecules, four of them with carboxylate oxygen atoms (O-H_{water}···O_{COO}) and the remaining four with carbonyl oxygen atoms (O-H_{water}···$O_{C=O}$) In addition, both compounds present two C-H···π interactions (Table 5).

The shape of the 2D fingerprint plots as well as the percentage of surface implied in each type of contact suggests very similar intermolecular interactions in **1** and **2**, either based on O_2H···O=C or O_2H···OOC hydrogen bonds (Tables 1 and 2) (S.I: Figure S14b). The main difference between the two compounds is observed in the "wings" zone[71] of the 2D fingerprint plot where the C-H··· π contacts are present. These interactions are also identified as flat regions in the curvedness mapping representation (S.I: Figure S14c). Moreover, the graphical representation of the intermolecular interactions of the Supporting Information shows that these contacts are nearer in **1** in comparison with **2**, with a 0.6% more surface implied in the C-H···C contacts (S.I: Figure S14d).

The Hirshfeld surface analysis of compounds **3** and **4** show H-bonds as the more important intermolecular interactions followed by weak C-H···O contacts (S.I: Figure 15a). In compound **3**, the H-bonds consist of four interactions between the amine units and the carbonyl oxygen atoms (N-H···$O_{C=O}$) and another four between the coordinated water molecules and the carboxylate oxygen atoms (O-H_{water}···O_{COO}). In addition, the C-H···O contacts are formed between the carbonyl moieties (eight contacts), carboxylate groups (four contacts) and coordinated water molecules (four contacts) acting as H-bond acceptors with *o*-H from the pyridyl and *p*-H from the phenyl rings of the 4-Phpy and the CH_3 groups of the ACA ligands acting as donors. In comparison, in compound **4**, the presence of the occluded EtOH molecules display two additional interactions between the amine moieties (N-H···O_{EtOH}) and another two with

carboxylate oxygen atoms ($O\text{-}H_{EtOH}\cdots O_{COO}$). Furthermore, the number of C-H···O contacts present in **4** is different in comparison with **3**, having eight interactions with carboxylate oxygen atoms ($C\text{-}H\cdots O_{COO}$), and four with carbonyl groups ($C\text{-}H\cdots O_{C=O}$) and water molecules ($C\text{-}H\cdots O_{water}$) as H-bond acceptors with *m*-H from the pyridyl and *o*-H and *m*-H from the phenyl rings of the 4-Phpy and *p*-H atoms from the ACA ligands acting as donors. Moreover, compound **3** presents two C-H···π intermolecular interactions which are not present in **4**, probably because of the disposition of the ligands in compound **4**, which only allows the formation of C-H··· π intramolecular interactions (Table 5).

Table 5. Comparison of the intermolecular interactions of compounds **1**-**4**.

Complex	D-H···A	Number of interactions	% of H···A contacts	Complex	D-H···A	Number of interactions	% of H···A contacts
1	$N\text{-}H\cdots O_{COO}$	4	14.4	**2**	$N\text{-}H\cdots O_{COO}$	4	14.5
	$O\text{-}H_{water}\cdots O_{COO}$	4			$O\text{-}H_{water}\cdots O_{COO}$	4	
	$O\text{-}H_{water}\cdots O_{C=O}$	4			$O\text{-}H_{water}\cdots O_{C=O}$	4	
	C-H···π	2	21.4		C-H···π	2	20.8
3	$N\text{-}H\cdots O_{C=O}$	4	6.7	**4**	$N\text{-}H\cdots O_{C=O}$	4	6.1
	$O\text{-}H_{water}\cdots O_{COO}$	4			$N\text{-}H\cdots O_{EtOH}$	2	
	$C\text{-}H\cdots O_{C=O}$	8			$O\text{-}H_{EtOH}\cdots O_{COO}$	2	
	$C\text{-}H\cdots O_{COO}$	4			$C\text{-}H\cdots O_{C=O}$	4	
	$C\text{-}H\cdots O_{water}$	4			$C\text{-}H\cdots O_{COO}$	8	
	C-H···π	4	35.1		$C\text{-}H\cdots O_{water}$	4	

The 2D fingerprint plots show two sharp peaks assigned to the H-bonds which are overlap with the C-H···O contacts in both compounds. Moreover, in compound **3**, the "wings" zone can be observed in the 2D fingerprint plot region while in compound **4**, these wings are not observed, suggesting the presence of close C-H···π contacts in **3** (S.I: Figure 15b). These planar interactions are also found in the curvedness representation, observing flat regions along the 4-Phpy ligands, where the C-H··· π contacts are observed while in the same representation of **4**, no clear flat regions are found (S.I: Figure 15c). In addition, the absence of planar interactions in **4** is supported by the graphical representation summarising the intermolecular interactions provided in

the Supporting Information (S.I: Figure 15d), with a 3.6% more surface implied in the C-H⋯ C contacts in **3**, probably caused by the contribution of the C-H··π interactions in this compound.

2.6. Thermogravimetric Analysis

Simultaneous TG-DTA determinations were carried out to evaluate the temperature where the occluded solvent molecules were lost and the thermal stability of compounds **3** (Figure 10) and **4** (S.I: Figure S16). The measurements were performed using 39.10 mg of **3** and 38.00 mg of **4**. Compound **3** starts to lose three occluded water molecules at 55ºC (weight loss exp. 6.5%, calc. 6.3%) until 93ºC. Then, between 93ºC and 180ºC the two coordinated water molecules are lost (weight loss exp. 4.2%, calc. 4.5%). From this temperature, the compound loses the two ACA ligands between 180ºC and 283ºC (weight loss exp. 47.9%, calc. 47.7%) and continues its decomposition ending at 425ºC. For compound **4**, the loss of the two occluded ethanol molecules starts at 75ºC (weight loss exp. 5.2%, calc. 5.3%) until 175ºC. Then, between 175ºC and 233ºC the compound loses two ACA ligands (weight loss exp. 24.4%, calc. 23.3%) and between 233ºC and 290ºC the remaining two ACA ligands (weight loss exp. 23.8%, calc. 23.3%). This difference of temperature in the loss of the ACA ligands could be promoted by the their different coordination modes. From 290ºC, the compound continues its decomposition ending at 425ºC.

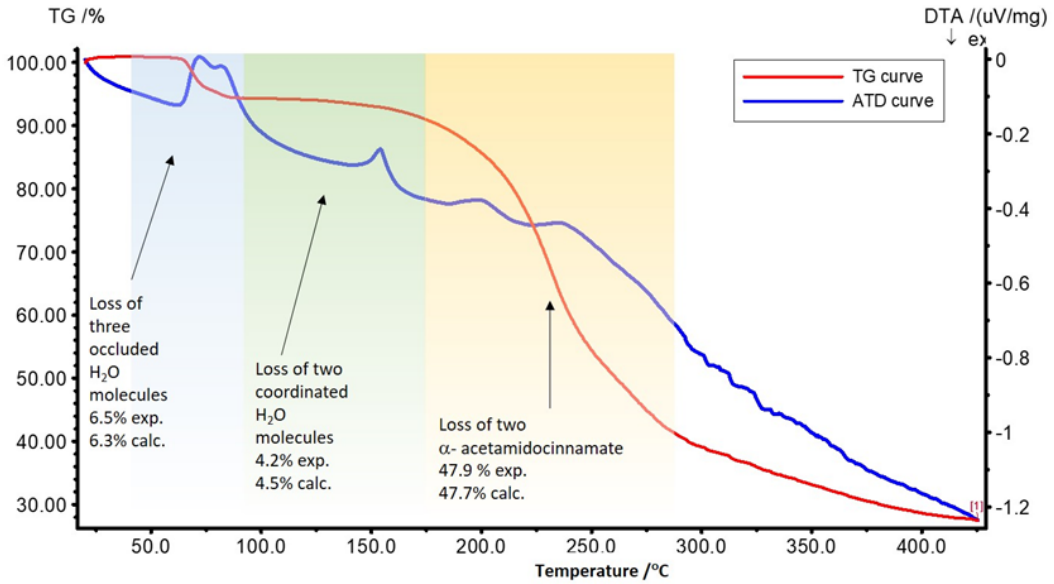

Figure 10. TG/DTA of compound $[Zn(4\text{-Phpy})_2(ACA)_2(H_2O)_2]\cdot 3H_2O$ (**3**) between 25ºC and 425ºC.

2.7. UV-Vis Spectroscopy and Photoluminescence Properties

The d orbitals' full population in d^{10} metal ions such as Zn(II) and Cd(II) only allows charge transfer (CT) transitions, either between the metal and the ligand or by the ligand itself (LMCT, MLCT and LLCT). These CTs between the π-π* orbitals are more energetic than those promoted by the d orbitals and thus fall into the UV region[72,73]. UV-Vis measurements were carried out for HACA, 4-Phpy and complexes **1-4** in a range of concentration from ~$1.00\cdot10^{-8}$ M to ~$1.00\cdot10^{-5}$ M. L-tyrosine has been used as reference for the calculation of the quantum yield. Their UV-Vis measurements have been carried out in a range of concentration from ~$1.00\cdot10^{-8}$ M to ~$1.00\cdot10^{-4}$ M for ascertaining the no aggregation effects of the samples at these concentrations (S.I: Figures S17 and S18). Complexes **1-4**, the free HACA acid and the 4-Phpy exhibit two different λ_{max} between 202-279 nm. Complex **4** presents the highest absorbance values while **2** displays the lowest (**4**>**1**>**3**>**2**). In addition, the absorption maximums of the complexes **1** (207 nm, 279 nm) and **2** (203 nm, 279 nm) are bathocromically shifted respect to the HACA acid (202 nm, 278 nm). By contrast,

complexes **3** (203 nm, 261 nm) and **4** (202 nm, 261 nm) present a bathocromical shift respect to the 4-Phpy ligand (202 nm, 256 nm) (S.I: Figure S19).

In previous research[74,75], we recorded the photoluminescence spectra of two Zn(II) and two Cd(II) complexes with Pip and 3-phenylpyridine (3-Phpy) or 4-Phpy ligands[74]. Moreover, the photoluminescence spectra of one Zn(II), two Cd(II) and one Hg(II) piperonylate compounds were measured and their quantum yields calculated[75]. As a continuation of this work, the photoluminescence properties of complexes **1**-**4** and HACA and 4-Phpy ligands have been measured at 298 K in EtOH solutions. Their emission spectra have been depicted in Figure 11. The photoluminescence emission spectra of the complexes have been carried out with an excitation wavelength of 275 nm. The photoluminescence measurements showed a bathochromic shift (342-348 nm) in emission of the complexes with respect to HACA (338 nm) and 4-Phpy (337 nm). These shifts could be promoted by the extending of the conjugation in the complexes[76,77].

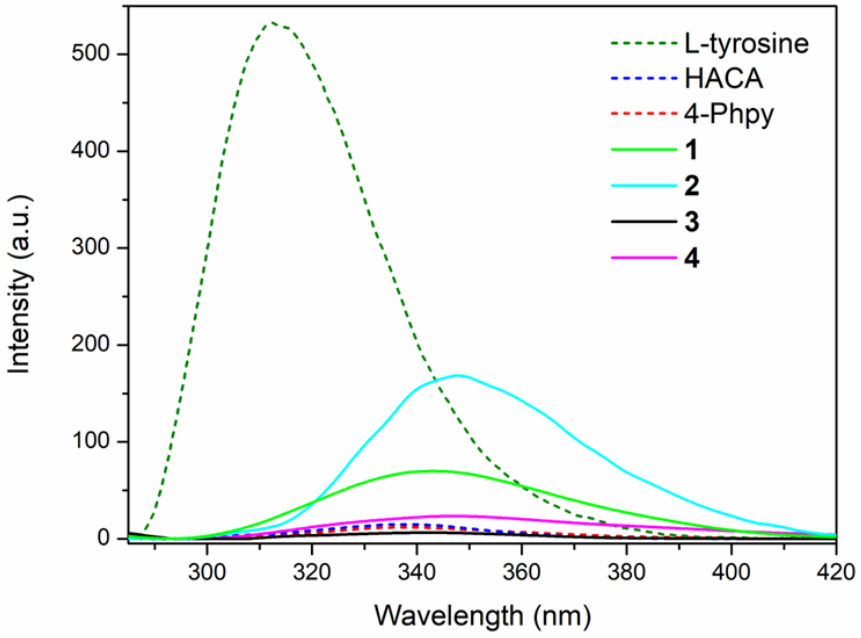

Figure 11. Emission spectra of complexes **1**-**4**, HACA and 4-Phpy ligands and L-tyrosine reference, excited at 275 nm at 298 K in Milli-Q water solution ($9.74 \cdot 10^{-6}$ M for L-tyrosine) or EtOH solutions ($5.00 \cdot 10^{-7}$ M for HACA, $3.80 \cdot 10^{-7}$ M for 4-Phpy, $4.97 \cdot 10^{-7}$ M for **1**, $3.77 \cdot 10^{-7}$ M for **2**, $3.01 \cdot 10^{-7}$ M for **3** and $1.10 \cdot 10^{-7}$ M for **4**).

Fluorescence quantum yield (φ) is defined as the ratio of the number of photons emitted to the number of photons absorbed and describes how a fluorophore converts the excitation light into fluorescence[78]. The relative fluorescence quantum yield is calculated relating the quantum yield value of the desired compound and comparing with a reference (standard)[79].

The quantum yields of compounds **1**-**4** as well as HACA and 4-Phpy have been calculated using equation 1,

$$\varphi_s = \varphi_r \left(\frac{OD_{ref}}{OD_s}\right)\left(\frac{I_s}{I_{ref}}\right)\left(\frac{n_s}{n_{ref}}\right)^2 \qquad \text{(eq. 1)}$$

where the quantum yields of the reference and the samples are φ_{ref} and φ_s, respectively. The equation also contains the area under the curve for the emission spectra (I), the optical density or absorbance (OD) and the refractive index of the solvent (n). Herein, L-tyrosine has been used as the standard (φ_{ref} = 0.14)[80] and the values of A_{ref} and I_{ref} have been obtained using a $9.74 \cdot 10^{-6}$ M solution with Milli-Q water as solvent (n_{ref} = 1.3325)[81] at 298 K. The values of A_s and I_s of complexes **1**-**4** and HACA and 4-Phpy have been measured in $4.97 \cdot 10^{-7}$ M (**1**)**,** $3.77 \cdot 10^{-7}$ M (**2**), $3.01 \cdot 10^{-7}$ M (**3**), $1.10 \cdot 10^{-7}$ M (**4**), $5.00 \cdot 10^{-7}$ M (HACA) and $3.80 \cdot 10^{-7}$ M (4-Phpy) solutions using EtOH as solvent at 298 K (n_s = 1.3608)[82]. The values of relative quantum yields obtained for compounds **1**-**4** are 0.019 (**1**), 0.037 (**2**), 0.0021 (**3**) and 0.0076 (**4**) (S.I: Table S1).

These results show that the coordination of the ACA ligand promotes an enhancement of the quantum yield when it is coordinated to Zn(II) and Cd(II) ions while the addition of the 4-Phpy displays a quenching effect, which reduce the quantum yield values. Despite these two effects, it seems that the quenching of the 4-Phpy is higher than the enhancement of the HACA and, therefore, compounds **3** and **4** present

very low quantum yield values. The calculated quantum yield values of the complexes are comparable to other compounds with d^{10} metal ions reported in the literature and could be promoted by their diversity on nuclearity, coordination modes and supramolecular structures[75,83,84].

3. Conclusions

In this paper, we present the reactions of $M(OAc)_2 \cdot 2H_2O$ (M = Zn(II) and Cd(II)) with HACA in EtOH as solvent yielding two isostructural monomeric complexes with octahedral M(II) geometries (**1** and **2**). These complexes have been used as precursors for the reaction with 4-Phpy, yielding compounds with different nuclearity depending on the metal centre. The reaction which starts from **1** yields a monomer (**3**), while the reaction starting from **2** results in a dimeric complex (**4**). The incorporation of the 4-Phpy ligand into the structure of **1** and **2** has changed the coordination modes of the ACA ligand (from chelate to monodentate in **1** and from chelate to bridge in **2**) without modifying the octahedral environment of the metal centers. In addition, a change in the disposition of the water molecules between compounds **1** and **3** has occurred, passing from *cis* to *trans*. These modifications in the structural arrays of the compounds may be justified because of the zero crystal field stabilization energy of Zn(II) and Cd(II), which favours the reorganization of the ligands by changing their coordination modes conserving the octahedral geometry of the corresponding metal centers.

The crystal structures of **1**-**4** have been elucidated, and their molecular and supramolecular interactions have been discussed. In addition, Hirshfeld surface analysis have been used to analyse the intermolecular interactions. The Hirshfield surface analysis allows us to confirm the stronger intermolecular interactions (H-bonds) of each

compound and also identificate the secondary intermolecular interactions (C-H···O and C-H···π interactions). Interestingly, the comparison of the Hirshfeld surfaces between **1** and **2** allows us to see the slighty difference between the intermolecular interactions of both compounds, which are the strength of their C-H···π interactions, probably produced by the different orientation of the ACA ligands in the complex due to the different ionic radii of Zn(II) and Cd(II).

Moreover, the thermal stability and the photoluminescence properties of the complexes have been analysed and their quantum yields calculated (**2**>**1**>**4**>**3**), observing and enhancement of the photoluminescence properties of the complexes with only ACA (**1** and **2**) and a quenching effect of the 4-Phpy in **3** and **4**, which could be caused by the low rigidity of this ligand as the different torsion angles suggest and the concomitant radiative decay.

4. Experimental Section

4.1. Materials and general details

Zinc(II) acetate dihydrate ($Zn(OAc)_2 \cdot 2H_2O$), cadmium(II) acetate dihydrate ($Cd(OAc)_2 \cdot 2H_2O$), α-acetamidocinnamic acid (HACA), 4-phenylpyridine (4-Phpy) and ethanol (EtOH) as solvent, were purchased from Sigma-Aldrich (Darmstadt, Germany). Deuterated dimethylsulfoxide (dmso-d_6) was used for the NMR experiments and was purchased from Eurisotop (Saint-Aubin, France). All of them were used without further purification. All the reactions and manipulations were carried out in air at room temperature (r.t.). Elemental analyses (C, H, N) were carried on a Euro Vector 3100 instrument. FTIR-ATR spectra were recorded on a Tensor 27 (Bruker) spectrometer, equipped with an attenuated total reflectance (ATR) accessory model MKII Golden Gate with diamond window in the range 4000-500 cm^{-1}. ^{1}H and $^{13}C\{^{1}H\}$ NMR spectra

were recorded on an NMR-FT Bruker 250, 360 and 400 MHz spectrometers in dmso-d_6 solution at r.t. All chemical shifts (δ) are given in ppm relative to TMS as internal standard. Simultaneous TG/DTA determinations for compounds **3** and **4** were carried out in a Netzsch STA 409 instrument, with an aluminium oxide powder (Al_2O_3) crucible and heating at 5 ºC·min^{-1} from 20 to 450 ºC, under a nitrogen atmosphere with a flow rate of 80 mL·min^{-1}. Al_2O_3 (Perkin-Elmer 0419-0197) was used as Standard. The electronic spectra in EtOH solution were run on an Agilent HP 8453 UV-Vis spectrophotometer with a quartz cell having path length of 1 cm in the range of 190-500 nm. Photoluminescence measurements were carried out with a Perkin Elmer LS 55 50 Hz Fluorescence Spectrometer using 1 cm quartz cell, in EtOH solution. The emission spectra were measured at 25 ºC. The samples were excited at 275 nm and the emission were recorded between 270-500 nm. The data obtained were corrected for the dilution effects by means of the Origin Pro 8.

*4.2 Syntheses of [Zn(ACA)$_2$(H$_2$O)$_2$] (**1**)*

An ethanolic solution (20 mL) of $Zn(OAc)_2{\cdot}2H_2O$ (150 mg, 0.683 mmol) was added dropwise to a solution of HACA (280 mg, 1.36 mmol) in EtOH (20 mL) as solvent at r.t. and stirred for 15 h until a white solid precipitate. The resulting solid was filtered and washed with 10 mL of cold EtOH. Suitable colourless crystals were obtained by slow evaporation of mother liquors in air for 3 days

Yield: 339 mg (97.3%) (respect to $Zn(OAc)_2{\cdot}2H_2O$). Elem. Anal. Calc. for $C_{22}H_{24}N_2O_8Zn$ (509.82 g·mol^{-1}) C 51.83; H 4.74; N 5.49. Found: C 51.59; H 4.65; N 5.32%. FTIR-ATR (wavenumber, cm^{-1}): 3298(m) [ν(N-H)], 3201-2782(br) [ν(O-H)]+[ν(C-H)$_{ar}$]+[ν(C-H)$_{alk}$]+[ν(C-H)$_{al}$], 1657(m) [ν(C=O)], 1643(m), 1561(s) [ν(C=C/C=N)], 1512(s) [ν_{as}(COO)], 1450(m), 1403(s) [ν_s(COO)], 1354(s)

[δ(C=C/C=N)], 1312(m), 1284(s) 1210(m), 1183(w), 1166(w), 1132(w), 1102(w), 1076(w), 1029(w), 1004(m) [δ_{ip}(C-H)], 980(w), 951(w), 912(w), 847(w), 793(m), 771(s) [δ_{oop}(C-H)], 754(s) [δ_{oop}(C-H)], 683(s) [δ_{oop}(C-H)], 597(s), 559(s), 527(m). ^{1}H NMR (400 MHz; dmso-d_6; Me_4Si; 298 K): δ = 9.18 [2H, s, N*H*], 7.51 [4H, d, ^{3}J = 7.3 Hz, *o-H*], 7.35 [4H, t, ^{3}J = 7.4 Hz, *m-H*], 7.29 [2H, d, ^{3}J = 7.1 Hz, *p-H*], 7.24 [2H, s, NH-C-C*H*], 1.95 [6H, s, CO-CH_3]. ^{13}C{^{1}H} NMR (360 MHz; dmso-d_6; Me_4Si; 298 K): 170.5 [NH-*C*O], 168.4 [*C*OO], 135.1 [OOC-*C*], 129.7 [HN-C-CH-*C*], 129.3 [*o-C*], 129.2 [*p-C*], 128.4 [*m-C*], 128.2 [NH-C-*C*H], 23.0 [CO-*C*H_3]. UV-Vis (EtOH): λ_{max} (log ε)= 207 (5.37), 279 nm (4.80). Photoluminescence (EtOH, $4.97 \cdot 10^{-7}$ M): λ_{ex} = 275 nm; λ_{em} (φ)= 343 nm (0.019).

*4.3 Syntheses of [Cd(ACA)$_2$(H$_2$O)$_2$] (**2**)*

An ethanolic solution (15 mL) of $Cd(OAc)_2 \cdot 2H_2O$ (152 mg, 0.569 mmol) was added dropwise to a solution of HACA (233 mg, 1.14 mmol) in EtOH (15 mL) as solvent at r.t. and stirred for 21 h until a white powder precipitated. The resulting solid was filtered and washed with 10 mL cold EtOH. Suitable colourless crystals were obtained by slow evaporation of mother liquors in air for 7 days.

Yield: 164 mg (51.8%) (respect to $Cd(OAc)_2 \cdot 2H_2O$). Elem. Anal. Calc. for $C_{22}H_{24}N_2O_8Cd$ (556.84 g·mol^{-1}) C 47.45; H 4.34; N 5.03. Found: C 47.23; H 4.19; N 4.88%. FTIR-ATR (wavenumber, cm^{-1}): 3272-3212(br) [ν(N-H)]+[ν(O-H)], 3082-2943(br) [ν(C-H)$_{ar}$]+[ν(C-H)$_{alk}$]+[ν(C-H)$_{al}$], 1657(m) [ν(C=O)], 1639(m), 1533(sh) [ν(C=C/C=N)], 1509(s) [ν_{as}(COO)], 1445(m), 1403(s) [ν_s(COO)], 1354(s) [δ(C=C/C=N)], 1309(m), 1286(m), 1206(m), 1178(w), 1162(w), 1127(w), 1102(w), 1074(w), 1029(w), 1002(m) [δ_{ip}(C-H)], 977(w), 948(w), 911(w), 844(w), 789(m), 773(s) [δ_{oop}(C-H)], 751(m) [δ_{oop}(C-H)], 680(s) [δ_{oop}(C-H)], 648(m), 637(m), 597(s),

544(s), 524(s). ^{1}H NMR (400 MHz; dmso-d_6; Me_4Si; 298 K): δ = 9.18 [2H, s, N*H*], 7.49 [4H, d, ^{3}J = 6.9 Hz, *o-H*], 7.35 [4H, t, ^{3}J = 7.4 Hz, *m-H*], 7.28 [2H, d, ^{3}J = 7.7 Hz, *p-H*], 7.26 [2H, s, NH-C-C*H*], 1.96 [6H, s, CO-CH_3]. $^{13}C\{^{1}H\}$ NMR (360 MHz; dmso-d_6; Me_4Si; 298 K): 171.5 [NH-*C*O], 168.2 [*C*OO], 135.2 [OOC-*C*], 129.5 [HN-C-CH-*C*], 129.3 [*o-C*], 129.1 [*p-C*], 128.3 [*m-C*], 128.1 [NH-C-*C*H], 23.1 [CO-*C*H_3]. UV-Vis (EtOH): λ_{max} (log ε)= 203 (5.80), 279 nm (4.87). Photoluminescence (EtOH, $3.77\cdot10^{-7}$ M): λ_{ex}= 275 nm; λ_{em} (φ)= 348 (0.037).

*4.4 Syntheses of [Zn(4-Phpy)$_2$(ACA)$_2$(H$_2$O)$_2$]·3H$_2$O (**3**)*

A hot ethanolic solution (40 mL) of **1** (100 mg, 0.197 mmol) was added dropwise to a solution of 4-Phpy (122 mg, 0.787 mmol) in EtOH (30 mL) as solvent at r.t. and stirred for 23 h. The resulting solution was concentrated under vacuum near dryness and kept on the fridge. After 1 day a white crystalline powder was obtained. The powder was filtered and washed with 10 mL of cold EtOH. Suitable colourless crystals for X-ray diffraction were obtained from the mother liquors on the fridge for 11 days.

Yield: 66.6 mg (39.5%) (respect to **1**). Elem. Anal. Calc. for $C_{44}H_{48}N_4O_{11}Zn$ (856.25 g·mol^{-1}) C 60.45; H 5.53; N 6.41. Found: C 60.48; H 5.27; N 6.32%. FTIR-ATR (wavenumber, cm^{-1}): 3383(w) [ν(O-H)], 3260(m) [ν(N-H)], 3092-2870(br) [ν(C-H)$_{ar}$]+[ν(C-H)$_{alk}$]+[ν(C-H)$_{al}$], 1681(m) [ν(C=O)], 1665(m), 1641(w), 1609(m) [ν_{as}(COO)], 1590(w), 1535(s) [ν(C=C/C=N)], 1505(m), 1486(s), 1446(w), 1417(m), 1392(s) [ν_{s}(COO)], 1352(s) [δ(C=C/C=N)], 1264(m), 1229(w), 1209(w), 1184(w), 1140(w), 1074(w) [δ_{ip}(C-H)], 1045(w) [δ_{ip}(C-H)], 1029(w), 1000(w), 980(w), 929(w), 836(m) [δ_{oop}(C-H)], 781(w), 762(s) [δ_{oop}(C-H)], 740(s), 730(s) [δ_{oop}(C-H)], 687(s), 650(m), 617(s), 609(s), 583(s), 555(s). ^{1}H NMR (360 MHz; dmso-d_6; Me_4Si; 298 K): δ

= 9.21 [2H, s, NH_{ACA}], 8.65 [4H, d, ^3J = 4.8 Hz, *o*-$H_{py,4\text{-}Phpy}$], 7.81 [4H, d, ^3J = 7.6 Hz, *o*-$H_{ph,4\text{-}Phpy}$], 7.74 [4H, d, ^3J = 5.0 Hz, *m*-$H_{py,4\text{-}Phpy}$], 7.52 [10H, m, *m*-$H_{ph,4\text{-}Phpy}$ + *p*-$H_{ph,4\text{-}Phpy}$+*o*-H_{ACA}], 7.35 [4H, t, ^3J = 7.1 Hz, *m*-H_{ACA}], 7.29 [2H, d, ^3J = 7.1 Hz, *p*-H_{ACA}], 7.25 [2H, s, NH-C-C*H*], 1.96 [6H, s, CO-CH_3]. $^{13}C\{^1H\}$ NMR (360 MHz; dmso-d_6; Me_4Si; 298 K): 168.4 [*C*OO,$_{ACA}$], 150.2 [*o*-$C_{py,4\text{-}Phpy}$], 147.6 [Ph-$C_{py,4\text{-}Phpy}$], 137.0 [Py-$C_{ph,4\text{-}Phpy}$], 135.0 [OOC-C_{ACA}], 129.6 [HN-C-CH-C_{ACA}], 129.5 [*o*-C_{ACA}], 129.3 [*m*-$C_{ph,4\text{-}Phpy}$ + *p*-$C_{ph,4\text{-}Phpy}$], 129.1 [*p*-C_{ACA}], 128.3 [*m*-C_{ACA}], 128.2 [NH-C-*C*H$_{ACA}$], 126.9 [*o*-$C_{ph,4\text{-}Phpy}$], 121.6 [*m*-$C_{py,4\text{-}Phpy}$], 23.1 [CO-*C*H$_{3,ACA}$]. UV-Vis (EtOH): λ_{max} (log ε) = 203 (6.20), 261 nm (4.51). Photoluminescence (EtOH, $3.01\cdot10^{-7}$ M): λ_{ex}= 275 nm; λ_{em} (φ)= 342 (0.0021).

*4.5 Syntheses of [Cd(4-Phpy)$_2$(μ-ACA)(ACA)]$_2$·2EtOH (**4**)*

A hot ethanolic solution (20 mL) of **2** (53.3 mg, 0.0957 mmol) was added dropwise to a solution of 4-Phpy (29.7 mg, 0.191 mmol) in EtOH (5 mL) as solvent at r.t. and stirred for 17 h. The resulting solution was concentrated under vacuum and kept on the fridge during 4 days until a white solid precipitate. The white solid was washed with 10 mL of cold EtOH. Suitable colourless crystals for X-ray diffraction were obtained keeping the mother liquors on the fridge for 3 days.

Yield: 58.3 mg (69.4%) (respect to **2**). Elem. Anal. Calc. for $C_{92}H_{88}Cd_2N_8O_{14}$ (1754.55 g·mol^{-1}) C 62.98; H 5.06; N 6.39. Found: C 62.74; H 4.98; N 6.18%. FTIR-ATR (wavenumber, cm^{-1}): 3291-3164(br) [ν(O-H)]+[ν(N-H)], 3078-3022(br) [ν(C-H)$_{ar}$]+[ν(C-H)$_{alk}$], 2975-2891(w) [ν(C-H)$_{al}$], 1672(s) [ν(C=O)], 1650(w), 1606(s), 1561(s) [ν_{as}(COO)], 1512(m) [ν_{as}(COO)], 1486(m) [ν(C=C/C=N)], 1445(w), 1387(s) [ν_s(COO)], 1347(m) [δ(C=C/C=N)], 1280(m), 1231(w), 1208(w), 1231(w), 1208(w), 1159(w), 1132(w), 1096(w), 1074(w) [δ_{ip}(C-H)], 1048(m) [δ_{ip}(C-H)], 1030(w),

1012(w), 981(w), 941(w), 923(w), 896(w), 837(w), 780(w), 762(s) [δ_{oop}(C-H)], 744(m), 731(s) [δ_{oop}(C-H)], 691(s), 619(m), 605(m), 561(m). ^{1}H NMR (250 MHz; dmso-d_6; Me_4Si; 298 K): δ = 9.18 [4H, s, NH_{ACA}], 8.64 [8H, d, ^{3}J = 5.7 Hz, *o*-$H_{py,4\text{-}Phpy}$], 7.81 [8H, d, ^{3}J = 6.6 Hz, *o*-$H_{ph,4\text{-}Phpy}$], 7.72 [8H, d, ^{3}J = 5.7 Hz, *m*-$H_{py,4\text{-}Phpy}$], 7.52 [20H, m, *m*-$H_{ph,4\text{-}Phpy}$+*p*-$H_{ph,4\text{-}Phpy}$ + *o*-H_{ACA}], 7.33 [16H, m, *m*-H_{ACA}, *p*-H_{ACA}+ NH-C-C*H*], 4.35 [2H, t, ^{3}J = 4.9 Hz, O*H*,$_{EtOH}$], 3.44 [4H, m, C$H_{2,EtOH}$], 1.96 [12H, s, CO-C$H_{3,ACA}$], 1.05 [6H, t, ^{3}J = 6.9 Hz, C$H_{3,EtOH}$]. ^{13}C{^{1}H} NMR (360 MHz; dmso-d_6; Me_4Si; 298 K): 171.4 [NH-*C*O$_{ACA}$] 168.1 [*C*OO,$_{ACA}$], 150.3 [*o*-$C_{py,4\text{-}Phpy}$], 147.4 [Ph-$C_{py,4\text{-}Phpy}$], 137.0 [Py-$C_{ph,4\text{-}Phpy}$], 135.2 [OOC-C_{ACA}], 129.6 [HN-C-CH-C_{ACA}], 129.4 [*o*-C_{ACA}], 129.3 [*m*-$C_{ph,4\text{-}Phpy}$ + *p*-$C_{ph,4\text{-}Phpy}$], 128.9 [*p*-C_{ACA}], 128.3 [*m*-C_{ACA}], 128.0 [NH-C-*C*H$_{ACA}$], 126.9 [*o*-$C_{ph,4\text{-}Phpy}$], 121.4 [*m*-$C_{py,4\text{-}Phpy}$], 56.1 [$CH_{2,EtOH}$], 23.1 [CO-*C*$H_{3,ACA}$], 18.6 [$CH_{3,EtOH}$]. UV-Vis: (EtOH) λ_{max} (log ε)= 202 (6.29), 261 nm (5.00). Photoluminescence (EtOH, $1.10\cdot10^{-7}$ M): λ_{ex}= 275 nm; λ_{em} (φ)= 347 (0.0076).

4.6. Crystallographic data

For compounds **1**-**4** a colourless prism-like specimen was used for the X-ray crystallographic analysis. The X-ray intensity data were measured on a D8 Venture system equipped with a multilayer mono-chromate and a Mo microfocus (λ = 0.71073 Å). For all compounds, the frames were integrated with the Bruker SAINT Software package using a narrow-frame algorithm. All hydrogen atoms were refined using a riding model (AFIX) with an isotropic temperature factor equal to 1.2, the equivalent temperature factor of the atom to which are linked and thus, the bond lengths of X-H were fixed. The structures were solved and refined using the Bruker SHELXTL Software package and refined using SHELX (version 2018/3)[85]. For **1**, the integration of the data using a monoclinic unit cell yielded a total of 26511 reflections to a maxim θ angle of 30.50º (0.70 Å resolution), of which 3376 were independent (average

redundancy 7.853, completeness = 99.9%), R_{int} = 5.15%, R_{sig} = 3.28%) and 2808 (83.18%) were greater than $2\sigma(F^2)$. The calculated minimum and maximum transmission coefficients (based on crystal size) are 0.6851 and 0.7461. For **2**, the integration of the data using a monoclinic unit cell yielded a total of 32182 reflections to a maxim θ angle of 30.56º (0.70 Å resolution), of which 3408 were independent (average redundancy 9.443, completeness = 99.2%), R_{int} = 2.46%, R_{sig} = 1.41%) and 3236 (94.95%) were greater than $2\sigma(F^2)$. The calculated minimum and maximum transmission coefficients (based on crystal size) are 0.7102 and 0.7461. For **3**, the integration of the data using a monoclinic unit cell yielded a total of 25967 reflections to a maxim θ angle of 26.41º (0.80 Å resolution), of which 4704 were independent (average redundancy 5.520, completeness = 99.0%), R_{int} = 3.50%, R_{sig} = 2.34%) and 4051 (86.12%) were greater than $2\sigma(F^2)$. The calculated minimum and maximum transmission coefficients (based on crystal size) are 0.7122 and 0.7454. For **4**, the integration of the data using a monoclinic unit cell yielded a total of 71093 reflections to a maxim θ angle of 26.38º (0.80 Å resolution), of which 8566 were independent (average redundancy 8.299, completeness = 99.8%), R_{int}= 10.32%, R_{sig} = 5.51%) and 6314 (73.71%) were greater than $2\sigma(F^2)$. The calculated minimum and maximum transmission coefficients (based on crystal size) are 0.6930 and 0.7454.

For **1**-**4**, the final cell constants and volume, are based upon the refinement of the XYZ-centroids of reflections above 2θ σ(I). Data were corrected for absorption effects using the Multi-Scan method (SADABS). Crystal data and relevant details of structure refinement for compounds **1**-**4**, are reported in Table 6. Molecular graphics were generated using Mercury 4.1.0 software[86,87] with POV-Ray Package[88]. Colour codes for all molecular graphics: dark blue (Zn), orange (Cd), red (O), light blue (N), dark grey (C) and white (H).

Table 6. Crystal data and structure refinement for **1-4**.

	1	**2**	**3**	**4**
Empirical Formula	$C_{22}H_{24}N_2O_8Zn$	$C_{22}H_{24}N_2O_8Cd$	$C_{44}H_{48}N_4O_{11}Zn$	$C_{23}H_{22}N_2O_{3.5}Cd_{0.50}$
Formula weight	509.80	556.83	874.23	438.62
T (K)	100(2)	100(2)	100(2)	100(2)
Wavelength (Å)	0.71073	0.71073	0.71073	0.71073
System, space group	Monoclinic, C2/c	Monoclinic, C2/c	Monoclinic, $P2_1/n$	Monoclinic, $P2_1/n$
Unit cell dimensions				
a (Å)	24.5715(9)	24.7566(10)	19.0159(8)	10.1812(4)
b (Å)	5.7176(2)	5.6126(2)	5.6182(2)	18.3797(7)
c (Å)	15.7610(6)	16.3388(6)	22.2031(10)	22.5622(9)
α (º)	90	90	90	90
β (º)	92.162(2)	98.895(2)	101.525(2)	96.9370(10)
ϒ (º)	90	90	90	90
V ($Å^3$)	2212.69(14)	2242.95(15)	2324.24(17)	4191.1(3)
Z	4	4	2	8
D_{calc} (mg/m^3)	1.530	1.649	1.249	1.390
μ (mm^{-1})	1.162	1.025	0.588	0.577
F (000)	1056	1128	916	1808
Crystal size (mm^{-3})	0.194x0.114x0.070	0.208x0.078x0.053	0.163x0.051x0.036	0.194x0.061x0.038
hkl ranges	-34<=h<=34, 8<=k<=8, 22<=l<=22	-35<=h<=35, 8<=k<=7, 23<=l<=23	-23<=h<=23, 7<=k<=6, 27<=l<=27	-11<=h<=12, 22<=k<=22, 28<=l<=28
2θ range (º)	2.586 to 30.500	2.801 to 30.558	2.579 to 26.406	2.300 to 26.379
Reflections collected/unique/[R_{int}]	26511/3376/ 0.0515	32182/3408/ 0.0246	25967/4707/ 0.0350	71093/8566/ 0.1032
Completeness to θ (%)	99.9	99.3	99.1	99.9
Absorption correction	Semi-empirical	Semi-empirical	Semi-empirical	Semi-empirical
Max. and min. transmission	0.7461 and 0.6851	0.7461 and 0.7102	0.7454 and 0.7122	0.7454 and 0.6930
Refinement method	Full-matrix least-square on F^2	Full-matrix least-square on F^2	Full-matrix least-square on F^2	Full-matrix least-square on F^2
Data/Restrains/Parameters	3376/5/161	3408/2/157	4704/3/285	8566/0/532
Goodness-on-fit on F^2	1.063	1.102	1.073	1.022
Final R indices [I>2σ(I)]	R_1 = 0.0309 wR_2 = 0.0614	R_1 = 0.0178 wR_2 = 0.0453	R_1 = 0.0514 wR_2 = 0.1518	R_1 = 0.0355 wR_2 = 0.0649
R indices (all data)	R_1 = 0.0455 wR_2 = 0.0659	R_1 = 0.0198 wR_2 = 0.0463	R_1 = 0.0598 wR_2 = 0.1603	R_1 = 0.0657 wR_2 = 0.0731
Extinction coefficient	n/a	n/a	n/a	n/a
Largest diff. peak and hole ($e.Å^{-3}$)	0.465 and -0.329	0.460 and -0.472	1.527 and -0.949	0.469 and -0.711

Conflicts

There are no conflicts to declare.

Acknowledgements

J. P. thanks CB615921 project, the CB616406 project from “Fundació La Caixa”, and the Generalitat de Catalunya (2017/SGR/1687). T. C. thanks the Spanish

National Plan of Research MAT2015-65756R. D. E. and F. S. acknowledges the PIF pre-doctoral fellowship from the Universitat Autònoma de Barcelona.

Appendix A. Supplementary data

CCDC 1979145-1979148 contain the supplementary crystallographic data for this paper. These data can be obtained free of charge via www.ccdc.cam.ac.uk/data_request/cif, or by emailing data_request@ccdc.cam.ac. uk, or by contacting The Cambridge Crystallographic Data Centre, 12 Union Road, Cambridge CB2 1EZ, UK; fax: +44 1223 336033.

References

[1] J. Singh, M. Yadav, A. Singh, N. Singh, Dalton Trans. 44 (2015) 12589–12597.
[2] K.Y. Zhang, G. Zeng, L.X. Sun, Y.H. Xing, F.Y. Bai, Inorg. Chem. 58 (2019) 15898–15908.
[3] L.J. Murray, M. Dincă, J.R. Long, Chem. Soc. Rev. 38 (2009) 1294–1314.
[4] D.R. Alcoba, O.B. Oña, G.E. Massaccesi, A. Torre, L. Lain, J.I. Melo, J.E. Peralta, J.M. Oliva-Enrich, Inorg. Chem. 57 (2018) 7763–7769.
[5] L. Ronconi, P.J. Sadler, Coord. Chem. Rev. 251 (2007) 1633–1648.
[6] J. Lee, O.K. Farha, J. Roberts, K.A. Scheidt, S.T. Nguyen, J.T. Hupp, Chem. Soc. Rev. 38 (2009) 1450–1459.
[7] J.J. Jiang, M. Pan, J.M. Liu, W. Wang, C.Y. Su, Inorg. Chem. 49 (2010) 10166–10173.
[8] S.A. Dalrymple, G.K.H. Shimizu, J. Am. Chem. Soc. 129 (2007) 12114–12116.
[9] J.J. Jiang, L. Li, M.H. Lan, M. Pan, A. Eichhöfer, D. Fenske, C.Y. Su, Chem. - A Eur. J. 16 (2010) 1841–1848.
[10] G. Beobide, O. Castillo, A. Luque, S. Pérez-Yáñez, CrystEngComm. 17 (2015) 3051–3059.
[11] Y. He, S. Xiang, B. Chen, J. Am. Chem. Soc. 133 (2011) 14570–14573.
[12] F. Hu, C. Liu, M. Wu, J. Pang, F. Jiang, D. Yuan, M. Hong, Angew. Chemie - Int. Ed. 56 (2017) 2101–2104.
[13] R. Carballo, B. Covelo, O. Gómez-Paz, A.B. Lago, E.M. Vázquez-López, Polyhedron 154 (2018) 398–406.
[14] Y. Yan, J. Huang, Coord. Chem. Rev. 254 (2010) 1072–1080.
[15] R.B. Lin, Y. He, P. Li, H. Wang, W. Zhou, B. Chen, Chem. Soc. Rev. 48 (2019) 1362–1389.
[16] S.A. Jenekhe, X.L. Chen, Science 283 (1999) 372–375.
[17] N. Hosono, S. Kitagawa, Acc. Chem. Res. 51 (2018) 2437–2446.
[18] H. Li, C.W. Hu, J. Solid State Chem. 177 (2004) 4501–4507.
[19] G.H. Wei, J. Yang, J.F. Ma, Y.Y. Liu, S.L. Li, L.P. Zhang, Dalton Trans. (2008) 3080–3092.
[20] O. Khalfaoui, A. Beghidja, J. Long, A. Boussadia, C. Beghidja, Y. Guari, J.

Larionova, Dalton Trans. 46 (2017) 3943–3952.
[21] S. Burt, Int. J. Food Microbiol. 94 (2004) 223–253.
[22] L. Liu, W.R. Hudgins, S. Shack, M.Q. Yin, D. Samid, Int. J. Cancer. 62 (1995) 345–350.
[23] F. Natella, M. Nardini, M. Di Felice, C. Scaccini, J. Agric. Food Chem. 47 (1999) 1453–1459.
[24] M. Kalinowska, R. Świsłocka, W. Lewandowski, J. Mol. Struct. 834–836 (2007) 572–580.
[25] G. Madhurambal, B. Ravindran, M. Mariappan, S.C. Mojumdar, J. Therm. Anal. Calorim. 100 (2010) 811–815.
[26] M. Puszyńska-Tuszkanow, W. Zierkiewicz, T. Grabowski, M. Daszkiewicz, G. Maciejewska, A. Adach, K. Kucharska-Ziembicka, J. Wietrzyk, B. Filip-Psurska, M. Cieślak-Golonka, J. Mol. Struct. 1134 (2017) 199–207.
[27] N. Bendjellal, C. Trifa, S. Bouacida, C. Boudaren, M. Boudraa, H. Merazig, Acta Crystallogr. Sect. C Struct. Chem. 74 (2018) 240–247.
[28] H.L. Wu, W.K. Dong, X.L. Wang, Zeitschrift Fur Krist. - New Cryst. Struct. 222 (2007) 36–38.
[29] A. Lehleh, A. Beghidja, C. Beghidja, R. Welter, M. Kurmoo, Comptes Rendus Chim. 18 (2015) 530–539.
[30] Λ.-Y. Fan, K. Li, X.-C. Huang, T. Sun, R.-R. Yun, H.-L. Wu, Zeitschrift Für Krist. - New Cryst. Struct. 224 (2014) 59–61.
[31] J.R. Allan, B.R. Carson, D.L. Gerrard, S. Hoey, Thermochim. Acta. 154 (1989) 315–322.
[32] I.E. Uflyand, V.A. Zhinzhilo, E.G. Drogan, D.A. Ostapenko, A.A. Novikova, V.E. Burlakova, G.I. Dzhardimalieva, J. Coord. Chem. 72 (2019) 796–813.
[33] J. Soldevila-Sanmartín, T. Calvet, M. Font-Bardia, C. Domingo, J.A. Ayllón, J. Pons, Dalton Trans. 47 (2018) 6479–6493.
[34] R. Chakrabarty, P.S. Mukherjee, P.J. Stang, Chem. Rev. 111 (2011) 6810–6918.
[35] J.M. Pan, Y.B. Ma, J. Shen, B. Liu, H. Liu, S.W. Jin, D.Q. Wang, J. Coord. Chem. 71 (2018) 2465–2486.
[36] X. Qing-Feng, Z. Qiu-Xuan, L. Jian-Mei, X. Xue-Wei, Z. Yong, J. Solid State Chem. 180 (2007) 207–212.
[37] G.B. Deacon, M. Forsyth, P.C. Junk, S.G. Leary, W.W. Lee, Z. Anorg. Allg. Chem. 635 (2009) 833–839.
[38] J. Yan, Y. Guo, H. Li, X. Sun, Z. Wang, J. Mol. Struct. 891 (2008) 298–304.
[39] W.C. Song, X.Z. Cui, X.G. Wang, L. Liang, E.C. Yang, X.J. Zhao, Polyhedron 127 (2017) 266–277.
[40] S.-F. Liu, Q. Wu, H.L. Schmider, H. Aziz, N.-X. Hu, Z. Popović, S. Wang, J. Am. Chem. Soc. 122 (2000) 3671–3678.
[41] J. Palion-Gazda, I. Gryca, A. Maroń, B. Machura, R. Kruszynski, J. Lumin. 192 (2017) 713–719.
[42] J. Li, J.H. Zhou, Y.Z. Li, L.H. Weng, X.T. Chen, Z. Yu, Z. Xue, Inorg. Chem. Commun. 7 (2004) 538–541.
[43] G.X. Liu, Y.Y. Xu, S. Nishihara, X.M. Ren, Russ. J. Coord. Chem. 36 (2010) 739–745.
[44] J. Zhang, S. Gao, C.M. Che, Eur. J. Inorg. Chem. (2004) 956–959.
[45] A. De, A. Sahu, S. Paul, M. Joshi, A.R. Choudhury, B. Biswas, J. Mol. Struct. 1167 (2018) 187–193.
[46] A. Erxleben, Coord. Chem. Rev. 246 (2003) 203–228.
[47] M. Borsari, Cadmium: Coordination Chemistry, Encycl. Inorg. Bioinorg. Chem.

(2014) 1–16.
[48] S. Das, P.K. Bharadwaj, Cryst. Growth Des. 6 (2006) 187–192.
[49] X.W. Wang, J.Z. Chen, J.H. Liu, Zeitschrift Fur Naturforsch. - Sect. B J. Chem. Sci. 62 (2007) 1139–1142.
[50] K. Nakamichi, K. Nabe, S. Yamada, T. Tosa, I. Chibata, Appl. Microbiol. Biotechnol. 19 (1984) 100–105.
[51] C.E. Song, Chem. Commun. (2004) 1033–1043.
[52] V.M. Rivera, J.P. Ruelas-Leyva, G.A. Fuentes, Catal. Today. 213 (2013) 109–114.
[53] G. B. Deacon;, R.J. Phillips, Coord. Chem. Rev. 33 (1980) 227–250.
[54] K. Nakamoto, Infrared and Raman Spectra of Inorganic and Coordination Compounds: Part A: Theory and Applications in Inorganic Chemistry, Wiley, 6th ed., Hoboken, New Jersey, USA, 2009.
[55] D.H. Williams; I. Fleming, Spectroscopic Methods in Organic Chemistry, McGrawHill, London, UK, 1995.
[56] P.M. Morse, G.S. Girolami, J. Am. Chem. Soc. 111 (1989) 4114–4116.
[57] J.C. Friese, A. Krol, C. Puke, K. Kirschbaum, D.M. Giolando, Inorg. Chem. 39 (2000) 1496–1500.
[58] H. Hosomi, S. Ohba, Y. Ito, Acta Crystallogr. Sect. C Cryst. Struct. Commun. 56 (2000) 123.
[59] S. Parshamoni, S. Konar, CrystEngComm. 18 (2016) 4395–4404.
[60] B.Y. Zhang, J.J. Nie, D.J. Xu, Acta Crystallogr. Sect. E Struct. Reports Online. 65 (2009) 880.
[61] S. Chooset, B. Cunningham, A. Kantacha, M. Zeller, S. Wongnawa, Acta Crystallogr. Sect. E Struct. Reports Online. 70 (2014) 106–107.
[62] H. Eshtiagh-Hosseini, H. Aghabozorg, M. Mirzaei, Acta Crystallogr. Sect. E Struct. Reports Online. 66 (2010) 882.
[63] A.C. Tella, J.A. Obaleye, M.D. Olawale, J.M. Vianney Ngororabanga, A.S. Ogunlaja, S.A. Bourne, Comptes Rendus Chim. 22 (2019) 3–12.
[64] S. Gao, Z. Fu, Z. Wang, Acta Crystallogr. Sect. E Struct. Reports Online. 63 (2007) 3004–3005.
[65] S. Tepavitcharova, D. Rabadjieva, D. Havlíček, I. Němec, P. Vojtíšek, J. Plocek, Z. Koleva, J. Mol. Struct. 1018 (2012) 113–121.
[66] B.D. Zdravkov, J.J. Čermák, M. Šefara, J. Janků, Cent. Eur. J. Chem. 5 (2007) 385–395.
[67] A.L. Spek, J. Appl. Crystallogr. 36 (2003) 7–13.
[68] G.G. Sezer, M. Arıcı, İ. Erucar, O.Z. Yeşilel, H.U. Özel, B.T. Gemici, H. Erer, J. Solid State Chem. 255 (2017) 89–96.
[69] P. Saxena, N. Thirupathi, Polyhedron 98 (2015) 238–250.
[70] S. K. Wolff, D. J. Grimwood, J. J. McKinnon, D. Jayatilaka and M. A. Spackman, CrystalExplorer, version 2.1; University of Western, Australia : Crawley, Australia, (2007).
[71] M.A. Spackman, J.J. McKinnon, CrystEngComm. 4 (2002) 378–392.
[72] J.E. Huheey, E.A. Keiter, R.L. Keiter, Inorganic chemistry: principles of structure and reactivity, 4th ed., HarperCollins College Publishers, New York, 1993.
[73] D. Sutton, Electronic Spectra of Transition Metal Complexes, McGraw-Hill, London, UK, 1975.
[74] M. Guerrero, S. Vázquez, J.A. Ayllón, T. Calvet, M. Font-Bardia, J. Pons, ChemistrySelect. 2 (2017) 632–639.

[75] D. Ejarque, F. Sánchez-Férez, J.A. Ayllón, T. Calvet, M. Font-Bardia, J. Pons, Cryst. Growth Des. 20 (2020) 383–400.
[76] E.L. Que, D.W. Domaille, C.J. Chang, Chem. Rev. 108 (2008) 1517–1549.
[77] A. Visscher, S. Bachmann, C. Schnegelsberg, T. Teuteberg, R.A. Mata, D. Stalke, Dalton Trans. 45 (2016) 5689–5699.
[78] S. Tarasi, A. Azhdari Tehrani, A. Morsali, P. Retailleau, New J. Chem. 42 (2018) 14772–14778.
[79] M.E. Sommer, M. Elgeti, P.W. Hildebrand, M. Szczepek, K.P. Hofmann, P. Scheerer, Structure-based biophysical analysis of the interaction of rhodopsin with g protein and arrestin, 1st ed., Elsevier Inc., Amsterdam, Netherlands, 2015.
[80] R.F. Chen, Anal. Lett. 1 (1967) 35–42.
[81] G.M. Hale, M.R. Querry, Appl. Opt. 12 (1973) 555–563.
[82] E. Sani, A. Dell'Oro, Opt. Mater. 60 (2016) 137–141.
[83] A. Sil, A. Maity, D. Giri, S.K. Patra, Sensors Actuators, B Chem. 226 (2016) 403–411.
[84] A. Das, S. Jana, A. Ghosh, Cryst. Growth Des. 18 (2018) 2335–2348.
[85] G.M. Sheldrick, Acta Crystallogr. A. 64 (2008) 112–122.
[86] C.F. Macrae, P.R. Edgington, P. McCabe, E. Pidcock, G.P. Shields, R. Taylor, M. Towler, J. van de Streek, J. Appl. Crystallogr. 39 (2006) 453–457.
[87] C.F. Macrae, I.J. Bruno, J.A. Chisholm, P.R. Edgington, P. McCabe, E. Pidcock, L. Rodriguez-Monge, R. Taylor, J. van de Streek, P.A. Wood, J. Appl. Crystallogr. 41 (2008) 466–470.
[88] Persistence of Vision Pty. Ltd. Persistence of Vision (TM) Raytracer; Persistence of Vision Pty. Ltd.: Williamstown, Australia, 2004; Available online: http://www.povray.org/